Supplemental Rear Wheel Power Steering System for a FSAE Vehicle

A Technical Report for MAE 4620

Presented to the Faculty of the School of Engineering and Applied Sciences
University of Virginia • Charlottesville, Virginia

In Partial Fulfillment of the Requirements for the Degree
Bachelor of Science in Mechanical Engineering

Author

Westin Recktenwald
May 10, 2021

Technical Project Team Members

Zackary Berman
Connor Greene
Lerene Palugod
Carolyn Wong

On my honor as a University Student, I have neither given nor received unauthorized aid on this assignment as defined by the Honor Guidelines for Thesis-Related Assignments

Signed: 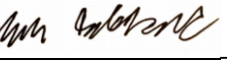 Date 5/10/2021
Westin Recktenwald
Approved _____ Date _____
Associate Professor Natasha Smith, Department of Mechanical and Aerospace Engineering

Background Information

The Formula SAE Competition

Formula SAE (FSAE) is a competition put on by SAE (Society of Automotive Engineers) International. It is an international, inter-collegiate student design competition that is centered around building and racing an open-wheeled, on-track race car much like the vehicle depicted in Figure 1 (Formula SAE, 2020, p. 5). This competition is made up of many different events held both on and off the track that aim to test different aspects of the vehicle to "[give] teams the chance to demonstrate their creativity and engineering skills in comparison to teams from other universities around the world" (Formula SAE, 2020, p. 5). For the competition's static events, teams compete in presentation, cost, and design events that test teams' abilities in business, budget, and engineering knowledge. The competition's dynamic events which include acceleration, skid pad, autocross, efficiency, and endurance focus on teams' physical vehicles and their design, manufacturing quality, and overall performance. This year, the University of Virginia (UVA) team will be competing in FSAE as Virginia Motorsports.

Figure 1: The University of Western Ontario team's FSAE car. This image shows the University of Western Ontario's FSAE car competing in the dynamic events at the 2014 Michigan FSAE competition (Brown, 2014).

Identification of Need

With the current setup of the vehicle, certain areas were marked for improvement based on what would help in the competition's events the most. Many of the competition's dynamic events such as the skid pad test and autocross event test vehicles' handling and stability through tight turns and high-speed cornering as seen in Figure 2 (Formula SAE, 2020). Based on this and the general length of the competition, the team marked three areas of need: reduce driver fatigue, faster steering response, and better handling and stability. The first area will help both with the aforementioned length, but also better allow the driver's senses to not be overwhelmed by turning in any dynamic event. The other two will help improve times and performance in the dynamic events, allowing a better overall performance of the vehicle itself. A supplemental rear wheel power steering system was determined to best improve the demonstrated needs of the current vehicle.

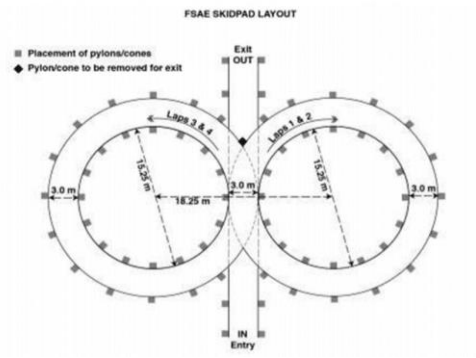

Figure 2: Skid pad test track layout. This image shows the track layout for the skid pad test where drivers will enter onto the track from the entrance at the bottom of the entrance, drive around the right-hand circle for two laps, turn and drive around the left-hand circle for two laps, and then exit the track using the exit shown at the top of the image. Since this track features continuous tight turns and teams are evaluated based on how fast they can complete this test, competing vehicles must be able to perform well under sustained high-speed cornering (Formula SAE, 2020, p. 127).

The Current Vehicle's Steering System

The current design of Virginia Motorsports' 2021 competition car's steering system is front steer with a rack and pinion. As shown in Figure 3, our vehicle's steering wheel is connected to the steering column using a universal joint. From there, the steering column actuates the pinion gear inside the vehicle's steering rack which, in turn, actuates the vehicle's front wheels via the attached tie-rods to turn them left or right depending on the driver's input at the steering wheel. The chosen rack and pinion for our vehicle is one by KAZ Technologies that weighs 3 lbs and features 248 degrees of pinion rotation for a total travel of 3.25 inches and a steering rack ratio of 4.71" per revolution (see Figure 4).

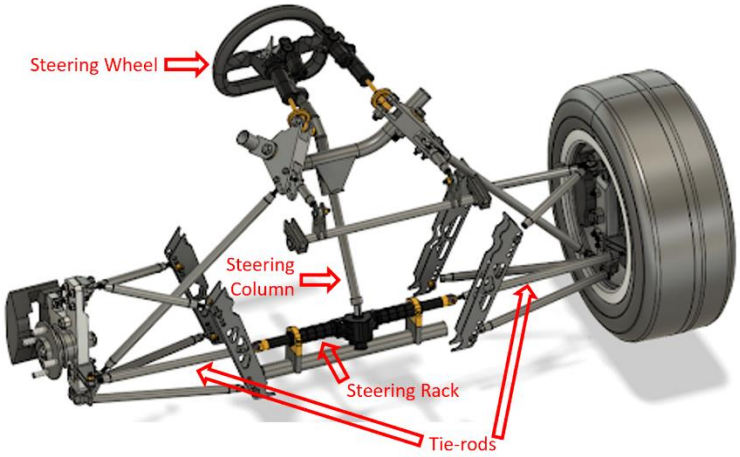

Figure 3: Virginia Motorsports' Front Steering System. This image depicts an isometric view of Virginia Motorsports' 2021 competition car's front steering system featuring the steering wheel, universal joint, steering column, steering rack, and tie-rods that work together to take driver input from the steering wheel and turn it into actuation of the front wheels.

Figure 4: KAZ Technologies Steering Rack. This picture is of the KAZ Technologies steering rack that Virginia Motorsports' will be using for their 2021 competition car's steering in the front (KAZ Technologies, 2014).

Designing a Supplemental Rear Wheel Power Steering System

Related FSAE Competition Rules

There are multiple rules related to front and rear FSAE steering that must be adhered to. As discussed in section V.3.2 of the 2021 FSAE competition rules, the car steering wheel must be mechanically connected to the front wheels, and electronic steering actuation of the front wheels is prohibited. Rear wheel steering may be implemented if desired, and electronic actuation of the rear wheels is allowed. If rear wheel steering is implemented, hard stops limiting the rear wheel steering travel to a maximum of 6 degrees are required. Lastly, steering fasteners are classified as "critical fasteners", and thus certain bolt and nut grades as well as positive fastener locking mechanisms are required (Formula 2020). All rules have been followed throughout the design process of the front and rear wheel steering systems.

System Performance Metrics

The system was designed to meet several performance metrics that would enable it to be effective throughout all of the conditions it would face. At the highest level regarding handling, the low speed effectiveness can be demonstrated by decreasing the turning radius by 20%. High-speed effectiveness can be demonstrated by a lane-change maneuver and comparing stability to when the system is turned off. This is intertwined with the ability to turn the wheels under the maximum force experienced by the tires. Furthermore, as dictated by the FSAE rules the system must have hard stops which limit the wheel travel to 6 degrees in either direction. For robustness, we also required that our system be able to return to zero as a fail-safe condition. Finally, the entire system must be under 12 pounds and be IP54+ waterproof and shockproof.

Narrowing down the Design

A decision matrix was created to select the device providing the steering force. The choices included an actuator (electronic, hydraulic, or pneumatic) or rack and pinion (electronic or hydraulic). The actuators were compared to each other based on their cost, weight, force output, control, ease of use and compactness. Each category was weighted differently, that is, their significance was not equal to each other. Points are assigned under each category based on the benefit provided by it. Points range from 0 - 2, where higher numbers offered greater benefit.

Table I

Decision Matrix for Method of Implementation for Supplemental Rear Wheel Power Steering

Categories	**Cost**	**Weight**	**Force Output**	**Control**	**Ease of Use**	**Compact-ness**	**Total**
Options **/weight**	**1**	**2**	**3**	**3**	**2**	**2**	
Electronic actuator	1	1	1	2	2	2	20
Hydraulic actuator	0	0	2	2	0	0	12
Pneumatic actuator	2	1	1	2	1	1	17
Electronic rack & pinion	1	2	1	0	2	1	14
Hydraulic rack & pinion	0	1	2	0	0	0	8

The design using independent linear electric actuators had the highest total number of points after calculations. As the most beneficial choice, it will be used in the final design.

Rear Steering Geometry Design

Determining the Vehicle's Desired Steering Performance

To understand the fundamentals of how a car equipped with four-wheel steering functions, it is necessary to understand steering geometry and tire deformation. When a vehicle turns, the outside wheels must travel a greater distance than the inside wheels due to the fact that the radius of the turn at the outside wheel is greater than the radius measured at the inside wheels. In its simplest form, steering geometry sketches are optimized to allow the vehicle to travel around a turn without dragging one or more wheels across the pavement due to the difference in turning radii between the outside and inside wheels (Milliken, 1995). When a steering geometry is designed such that all four wheels rotate about the same central point of the turn, a 100% Ackerman geometry is achieved as shown in Figure 5.

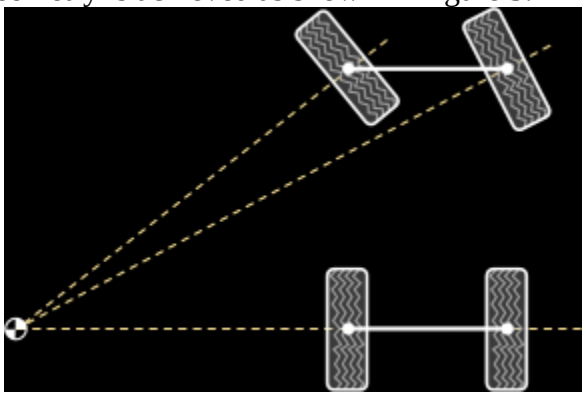

Figure 5: 100% Ackerman Steering Geometry (Ackerman Steering, 2016).

Greater complexity is introduced when the elastic deformation of the polymer tires due to the normal, lateral, and longitudinal loads on the tires is considered by the steering geometry. When a car travels around a turn, the outside wheels will be loaded more heavily than the inside

wheels due to the force acting at the car's center of gravity due to the centrifugal acceleration experienced by the car. Under this higher load, the outside wheels deform more than the inside wheels. This causes the car's instantaneous center of rotation about each wheel to be different than a steering geometry not accounting for dynamic tire deformation would predict. Steering geometries used to account for tire deformation include Parallel and Anti-Ackerman geometries. In short, these geometries simply cause the outside wheel of the car to turn significantly more than the inside wheel, thus creating a common center point of rotation for the car when the outside wheels have deformed more than the inside (McRae, 2019). Parallel and Anti-Ackerman front wheel steering geometries are shown in parts b and c of Figure 6.

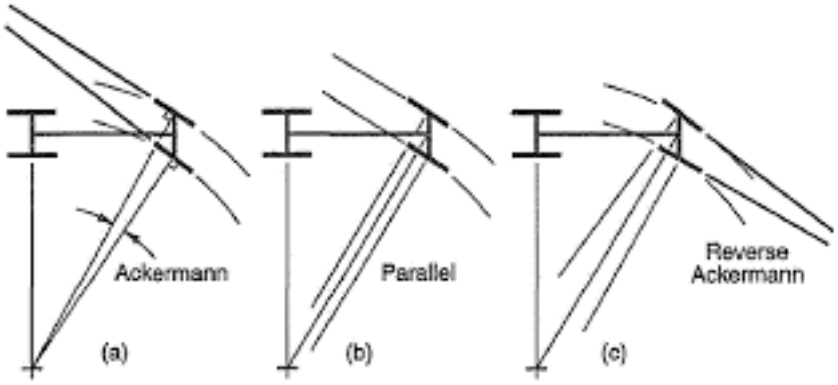

Figure 6: Ackerman, Parallel, and Anti-Ackerman Steering Geometries (Milliken, 1995).

Rear wheel (also referred to as four wheel) steering geometries require very similar design considerations as front wheel steering geometries. The significant new complexity involved in rear wheel steering geometry is that at low speeds, the rear wheels are turned in the opposite direction as the front wheels, and at high speeds, all four wheels are turned in the same direction as shown in Figure 7. This is done to achieve the shortest possible turning radius at low speeds and improve maneuverability at high speeds (Sparrow et al., 2016).

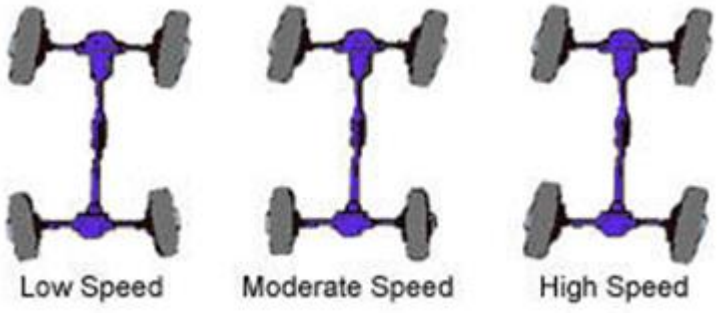

Figure 7: Speed dependent rear wheel steering (General Motors Quadrasteer Technology, n.d.).

Steering Geometry Decisions and Master Sketches

For the FSAE rear wheel steering designed for this project, a negative 100% Ackerman steering geometry is implemented at low speeds, and a positive Parallel steering geometry is to be implemented at high speeds. Due to the insignificant tire deformation induced at low speeds and the significant tire deformation induced at high speeds, Ackerman and Parallel rear steering geometries are implemented at low and high speeds, respectively. While ideally the rear wheels are turned at the same angle as the front wheels at low speeds to achieve the smallest turning

radius geometrically possible (Arvind, 2013), the FSAE rules limitation of 6 degrees of maximum rear wheel travel constrains the allowable rear wheel angular travel to 6 degrees. The following CAD screenshots, Figure 8 and Figure 9, illustrate our FSAE car's four-wheel steering geometry.

Figure 8: Virginia Motorsports' FSAE car's low speed negative rear wheel steering with 100% Ackerman rear geometry.

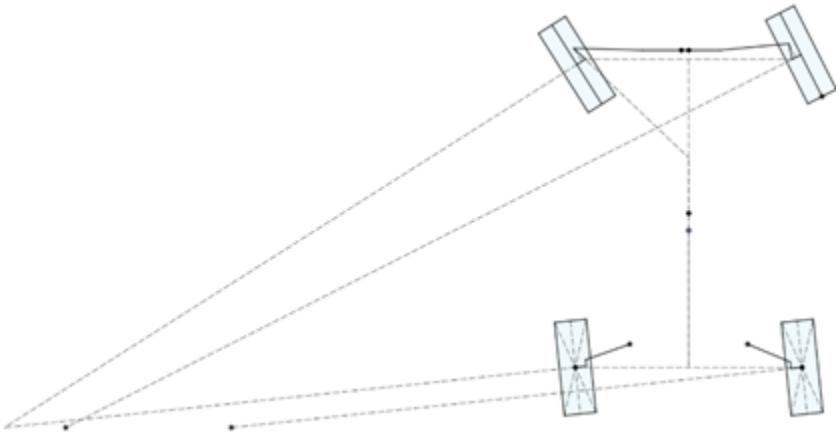

Figure 9: Virginia Motorsports' FSAE car's high speed positive rear wheel steering, Parallel rear geometry.

Examining the rear wheels more closely in Figure 10, the point circled in orange represents the steering tie rod's connection to the suspension upright. The point circled red represents the steering tie rod's connection to the RWS rocker. As the rear wheels are steered by driving the front steering rack position, the change in length of the rear tie rod directly corresponds to the change in length of the linear actuator needed to achieve the desired rear wheel angle.

Bump Steer Analysis

A vehicle's suspension system is simply a set of mechanical linkages. As such, they prescribe certain paths of motion in 3D space during suspension travel. The exact path the suspension will travel is a function of the many suspension parameters that define the location of the suspension linkages in space. As the rear suspension travels up and down due to bumps, potholes, and other dynamic driving scenarios, it is critical that the tires do not steer in or out as it travels. An unintended steering motion of the tires during the suspension travel is a product of a poorly optimized suspension geometry and can create very unpredictable and undesirable vehicle handling characteristics. Therefore, the suspension geometry must be optimized to ensure

that steering of the tire due to suspension travel is minimized to a negligible magnitude. As shown in Figure 10, this optimization is done in the front view of the geometry. This front view CAD sketch shows the centerline of the wheel and well as the upper and lower ball joints and frame mounts. The suspension in this sketch is traveled up and down by redefining the dimension representing ground clearance. As the suspension is traveled, the length of the tie rod, which connects the suspension upright to the rear steering system's rocker, changes slightly (this dimension is boxed in green in Figure 10). Because in reality the tie rod is a solid steel tube that does not change length, this geometric "change in length" of the tie rod manifests itself as change in the rear tire's steering angle. The position of the tie rod's mounting points, both at the suspension upright and the rear steering rocker is optimized by iterating through many different possible mounting locations and checking which locations amount to the lowest magnitude of bump steer. After optimization, the total "change in length" of the tie rod due to the full 2.5" of rear suspension travel is 0.01" for our suspension geometry. This small change in tie rod length produces a negligible change in tire steering angle throughout the suspension's full travel.

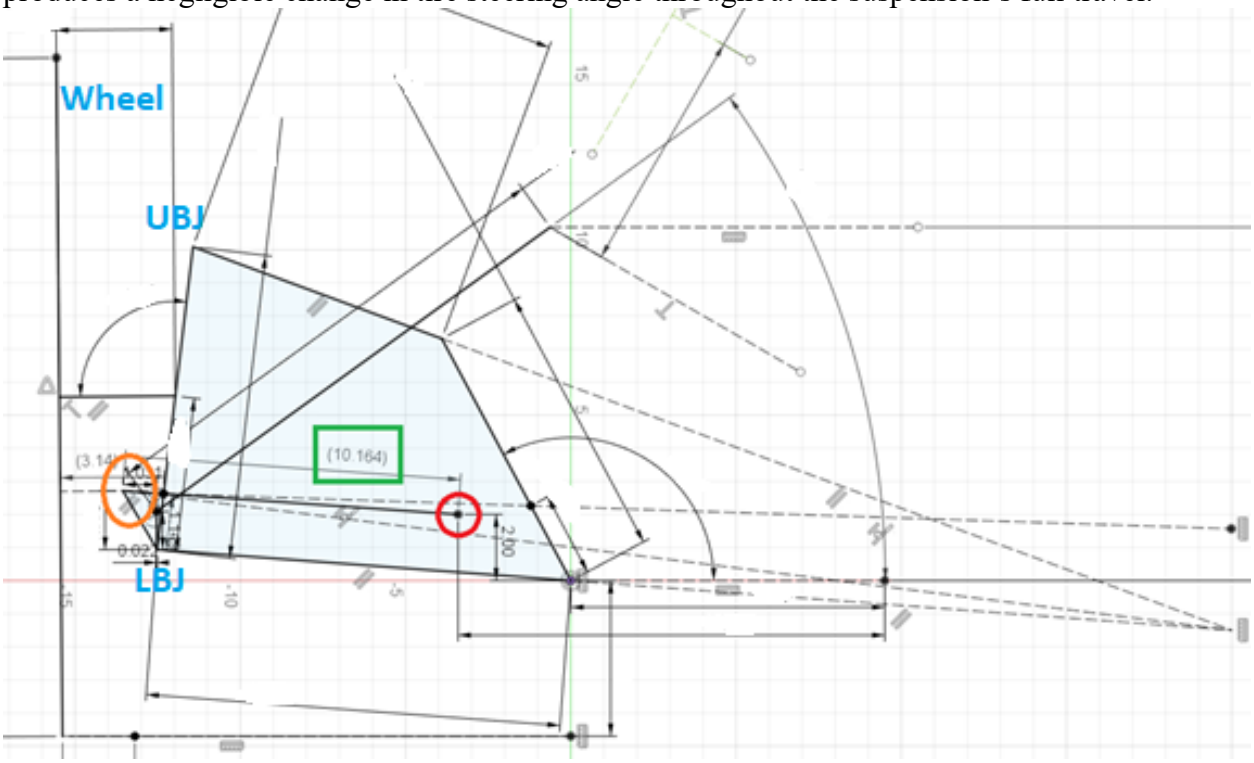

Figure 10: Virginia Motorsports' FSAE car's RWS bump steer analysis. Side view of suspension geometry shown.

For context of how the side view relates to the top view of the geometry, Figure 10 shows the mounting point of the rear tie rod at the rear steering rocker in red and the mounting (the point circled in orange in Figures 10 and 11).

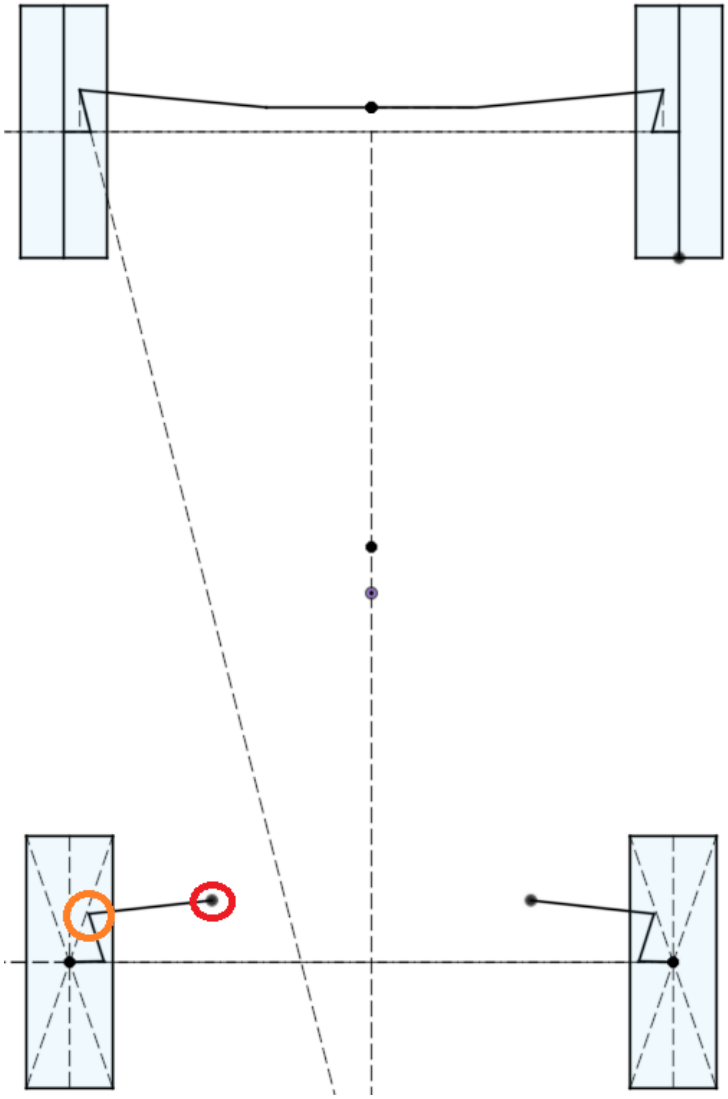

Figure 11: Virginia Motorsports' FSAE car's top down view of rear wheels. Tie rod outboard link circled in orange, inboard link circled in red.

Mechanical Design Overview

Analyzing the System's Loads in terms of Vehicle Performance

Tire performance is critical to understanding how a vehicle will perform because tires are the only contact that a vehicle has with the road surface. Creating grip with these contact patches allows vehicles to turn around corners, accelerate, and brake. Under load, a tire creates lateral friction through a phenomenon called "slip", in which the angle of the tire is different from the direction of its travel. This creates deformation of the sidewall, and the reaction force of this deformation gives grip to the vehicle. Fundamentally, a steering system counteracts a moment around the centerline of a tire. In most cases, the contact patch of a tire acts away from the centerline of the wheel, which creates this moment referred to as the pneumatic trail.

Choosing the correct actuator was one of the most important decisions made by the team, so it was critical to have data to back it up. Tire performance data obtained from the FSAE tire

test consortium (FSAETTC) allowed us to determine the maximum force our actuator would experience. The conditions of one test matched those that would be experienced by our car under hard cornering. The results are shown in Figure 12, which indicate a maximum aligning moment of 98.9 N*m.

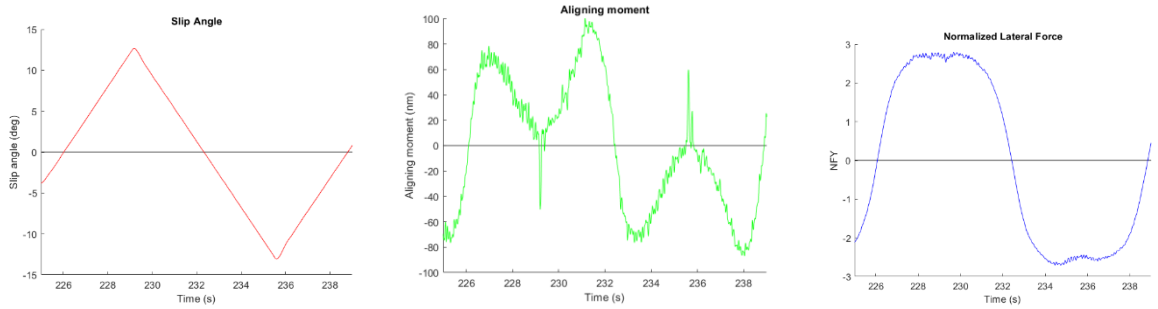

Figure 12: Coefficient of friction and Aligning moment with respect to slip angle.

Combining this information with a variable steering arm length, we were able to find the force required and thus create the decision matrix for the actuator.

Choosing the System's Components

As previously discussed, a decision matrix on the type of actuator determined an electronic actuator to be the most beneficial. In order to determine the best actuator for doing the job, market research was done to see what was available, which was then trimmed down using the specifications as listed in the *System Performance Metrics* section as applicable. It was found that actuators capable of mid-range forces, approximately 200 lbf, that had a built in potentiometer or encoder would be ideal. Issues arose surrounding the speed required of the actuator in order to provide a decent response time to driver input. After modification of the original mounting intent, an actuator was decided that was able to fix these problems. The team settled on the Linear Actuator PA-03 by Progressive Automations, which with proper packaging are able to quickly actuate through the full allowed range of motion of the rear wheels (*Linear Actuator PA-03*, n.d.).

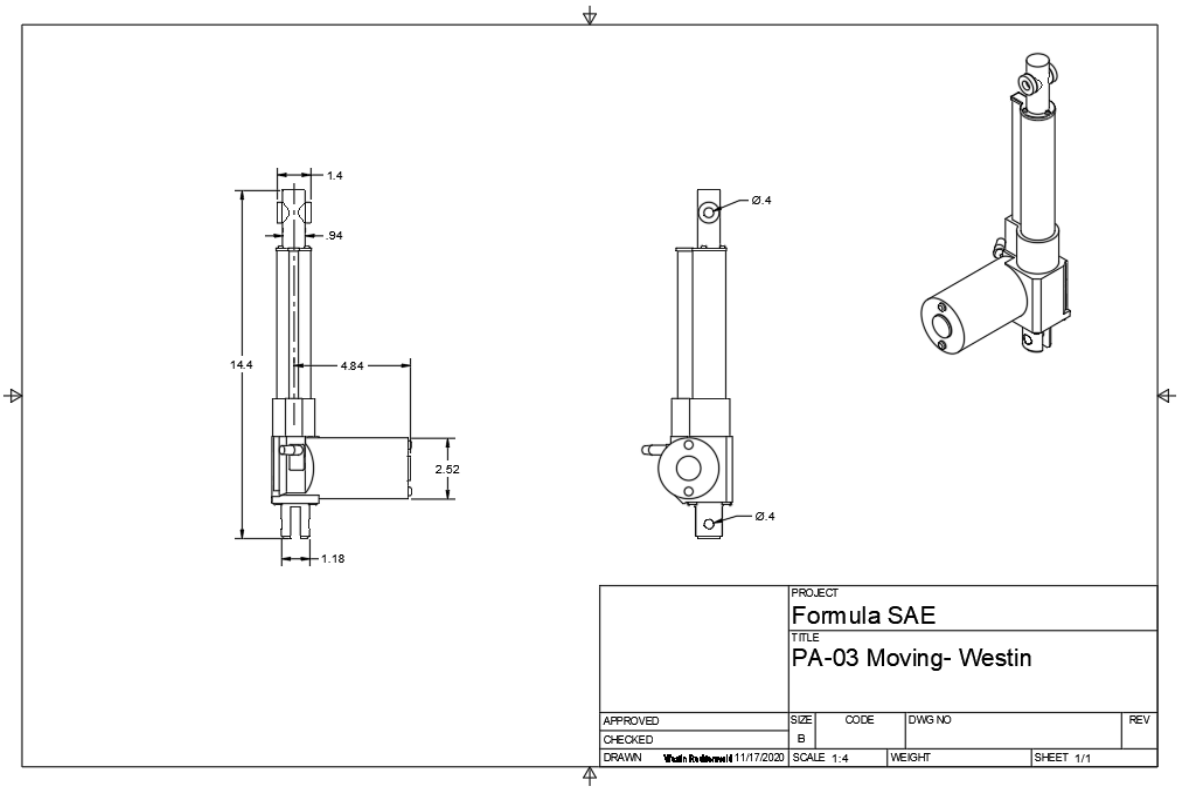

Figure 13: Dimensioned PA-03 actuator, unextended.

Figure 14: Image of PA-03 linear actuator (*Linear Actuator PA-03*, n.d.).

Another decision matrix was created to decide the type of sensor to use for data acquisition. The choices included an encoder, potentiometer or strain gauge. They were compared to each other based on cost, the accuracy of the data produced and whether there was much noise as well as ease of use. This decision matrix followed the same format as the one for actuator type (see Table II). The potentiometer had the highest total number of points and was selected for the design. Choosing a specific potentiometer was simple, because its travel needed to be matched to the steering column's travel of 248 degrees. A resistance of at least 1 kOhm was necessary to be compatible with the board voltage, and it needed to be mountable to our steering rack. Our final choice was the KAZ Technologies Steering Angle Sensor, a

potentiometer that met all the above mentioned needs as it is designed for the steering rack the team used. As a result, this potentiometer would be easy to mount and have enough resolution for our steering rack's actuation.

Table II

Decision Matrix for Data Acquisition Sensors

Categories	**Cost**	**Noise**	**Accuracy**	**Ease of Use**	**Total**
Options/**weight**	**1**	**2**	**2**	**3**	
Encoder	0	2	2	1	11
Potentiometer	2	0	2	2	12
Strain gauge	1	1	1	0	5

The hall effect sensor was an even simpler selection as it only needed to read a digital signal for the vehicle's speed. Our choice was the 7674K25 from McMaster-Carr with an input voltage range from 15V - 34V and a max current of 150mA. This hall effect sensor was deemed more durable and robust than other options considered, and was easy to mount on the current setup. The presence of the castle teeth on the vehicle's half shafts will provide a sufficient magnetic field to activate the sensor's detection.

Encoder Analysis and Choice

Because the linear actuator's motor we chose does not have any motor feedback (such as a motor encoder), the linear actuator's position is not directly known and therefore cannot be used to calculate the rear wheel's steering angle. Thus, a sensor must be integrated into the system to provide the information necessary to calculate the wheel's steering angle. Specifically, a linear potentiometer or linear encoder could be mounted in line with the linear actuator, thus effectively yielding the needed information in the form of the linear actuator's change in length over time. This method of sensing was not pursued due to the high cost of a linear potentiometer or encoder with the needed accuracy. Alternatively, a rotary potentiometer or rotary encoder could be mounted in line with the steering rocker's central pivot. In this orientation, the rotary sensor measures the steering rocker's angle, which can be used to directly calculate the rear wheel's steering angle. The rotary encoder mounted in line with the pivot of the rocker's axis of rotation, as shown in Figure 15, was ultimately chosen due to ease of mounting and because the encoder chosen provided the high accuracy needed.

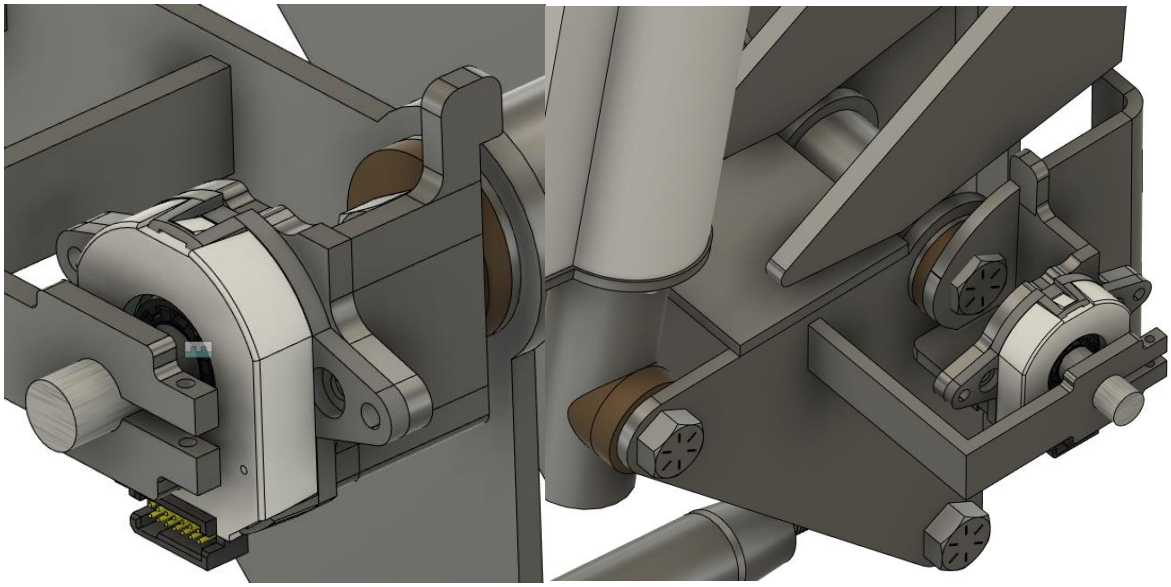

Figure 15: Virginia Motorsports' FSAE car's rotary encoder and encoder mounting.

The rotary sensor's resolution necessary for desirable system performance was determined by first by using the CAD assembly of the system to determine the actuator's total length of travel necessary to actuate the wheel to ±6° of steer. After knowing that the actuator must travel a total of 0.84", the steering rocker angles corresponding to maximum right and left steering directions were determined using the rear steering geometry. The total travel of the steering rocker is 16.36°. Therefore, the rocker (and thus rotary sensor) rotates 1.36° for every one degree of wheel steering angle (16.36/12 = 1.36°). To determine the sensor resolution needed, it was necessary to decide that inaccuracies in less than 0.1° of wheel steering angle would be unperceivable to the vehicle's driver and would cause no tangible change in vehicle performance. Thus, the minimum number of pulses per revolution of the rotary encoder is 2678 PPR (1.36°10365°rev=2678 PPR). The rotary encoder chosen for our project was the AMT 203-V.

Hall Effect Sensor Choice and Mounting

The hall effect sensor needed to be mounted close to the rear axle's castle ring to receive the signal necessary to calculate wheel speed. To hold the hall effect sensor in a desirable location, a sheet metal bracket was designed that allows the sensor's position relative to the castle ring to be adjusted in order to ensure optimal sensing accuracy. This sheet metal bracket bolts onto the rear suspension upright using one of the same bolts that holds the brake caliper mount to the opposite side of the upright. This is shown in Figure 16.

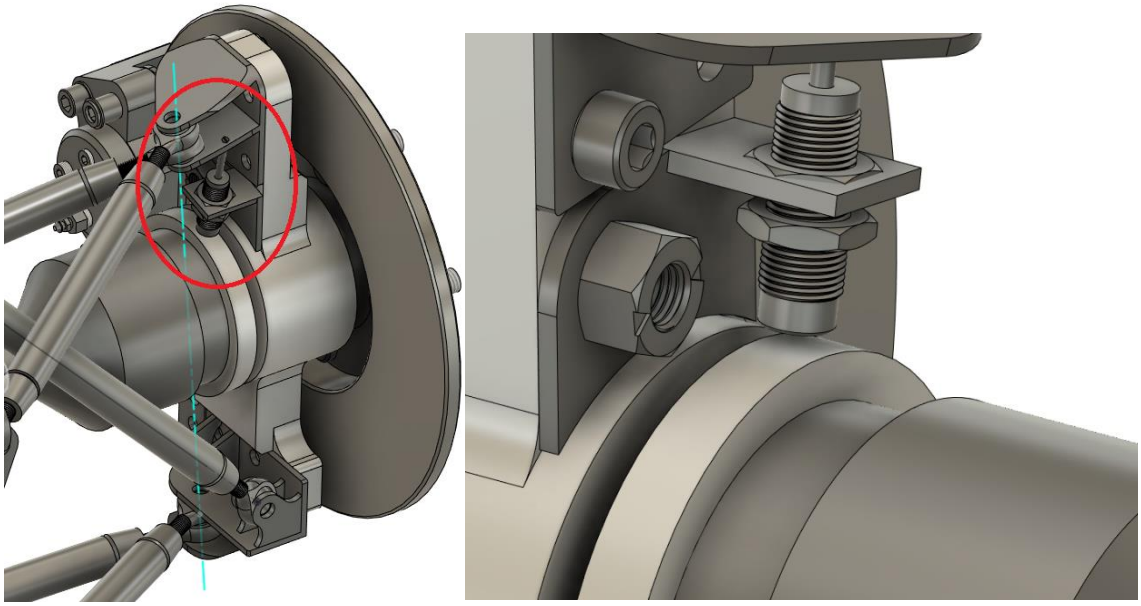

Figure 16: Virginia Motorsports' FSAE car's hall effect sensor mounting.

Mounting the Actuators

Packaging the actuators proved to be one of the most challenging aspects of the system's mechanical design. The trade-off between size of an actuator and the power it is capable of producing greatly affects the placement of its mounting points: smaller actuators require a longer steering arm to overcome the torque, but may not have the speed that is required for matching driver input. Since the team decided that a large and fast actuator was needed to meet the design requirements, a suitable mounting position directly to the steering arm could not be found. To overcome this a "remote" mounting system was devised so that the actuator could be located in a more desirable position. Taking cues from the inboard suspension which uses a pushrod and rocker to translate linear motion, a similar system was devised for the actuator. Figure 17 shows the subsystem with the actuator, rocker, and pushrod attached to the frame tabs and upright. Figures 18, 19, and 20 show dimensioned drawings of the rocker, tie rod, and their dimensioned placement in the overall system respectively. It is important to note that the rocker has a 1:1 ratio which means it provides a direct force translation from the vertical direction to the horizontal.

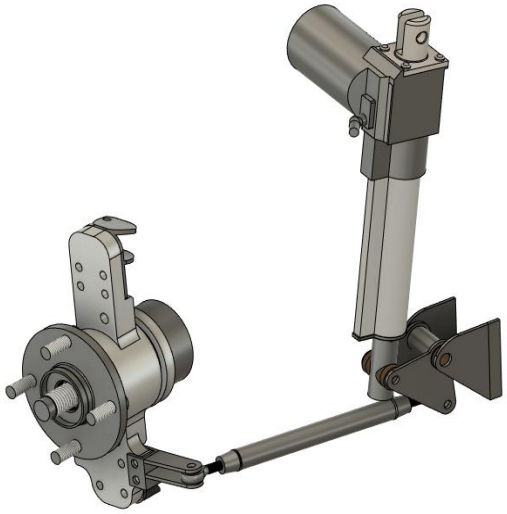

Figure 17: RWS subsystem CAD model.

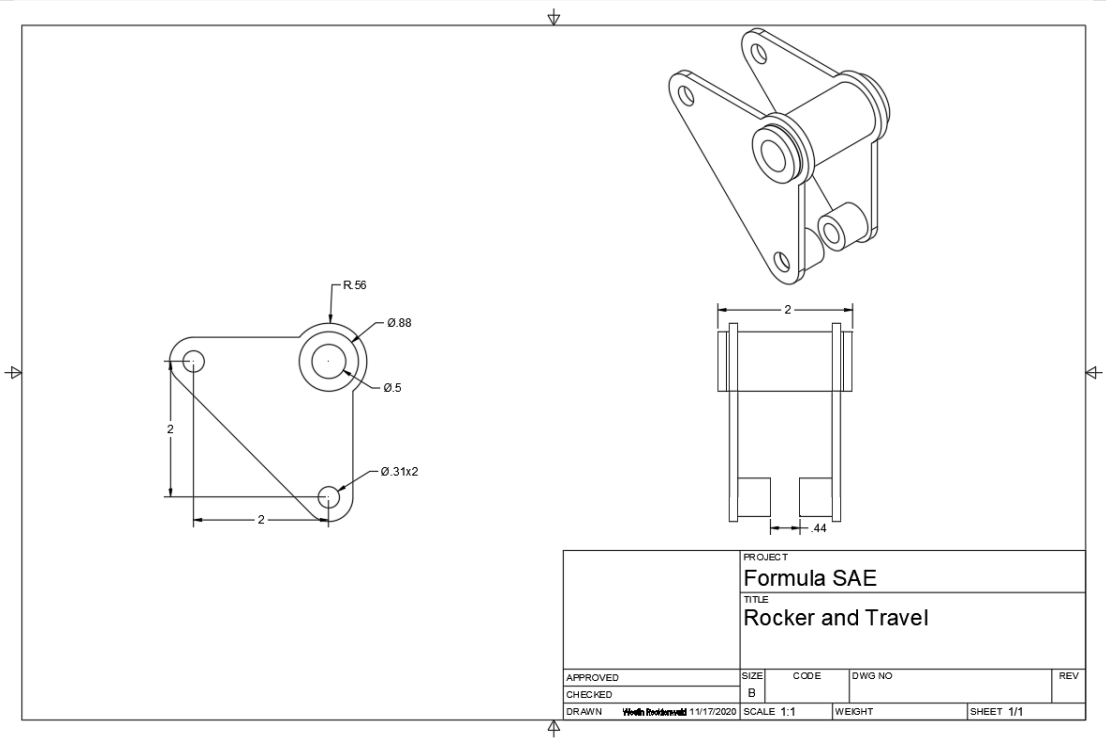

Figure 18: Dimensioned Drawing of Rocker in RWS subsystem.

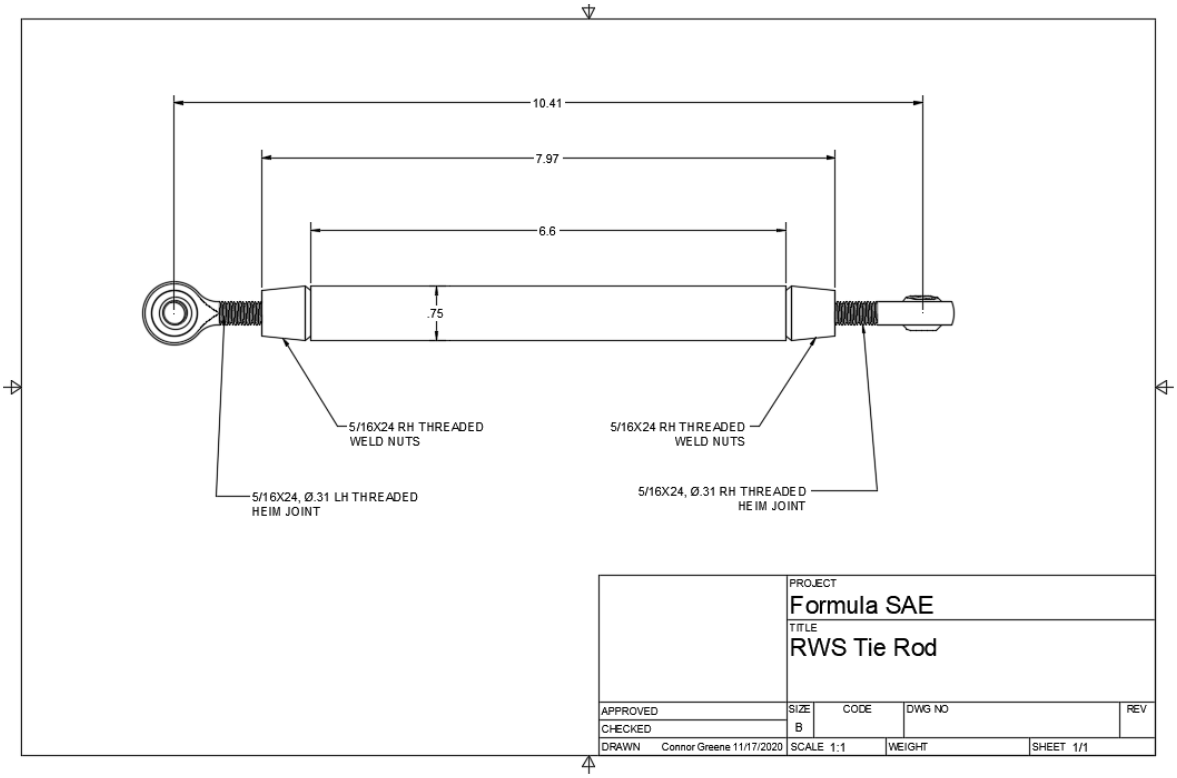

Figure 19: Dimensioned Drawing of Tie-Rod in RWS subsystem.

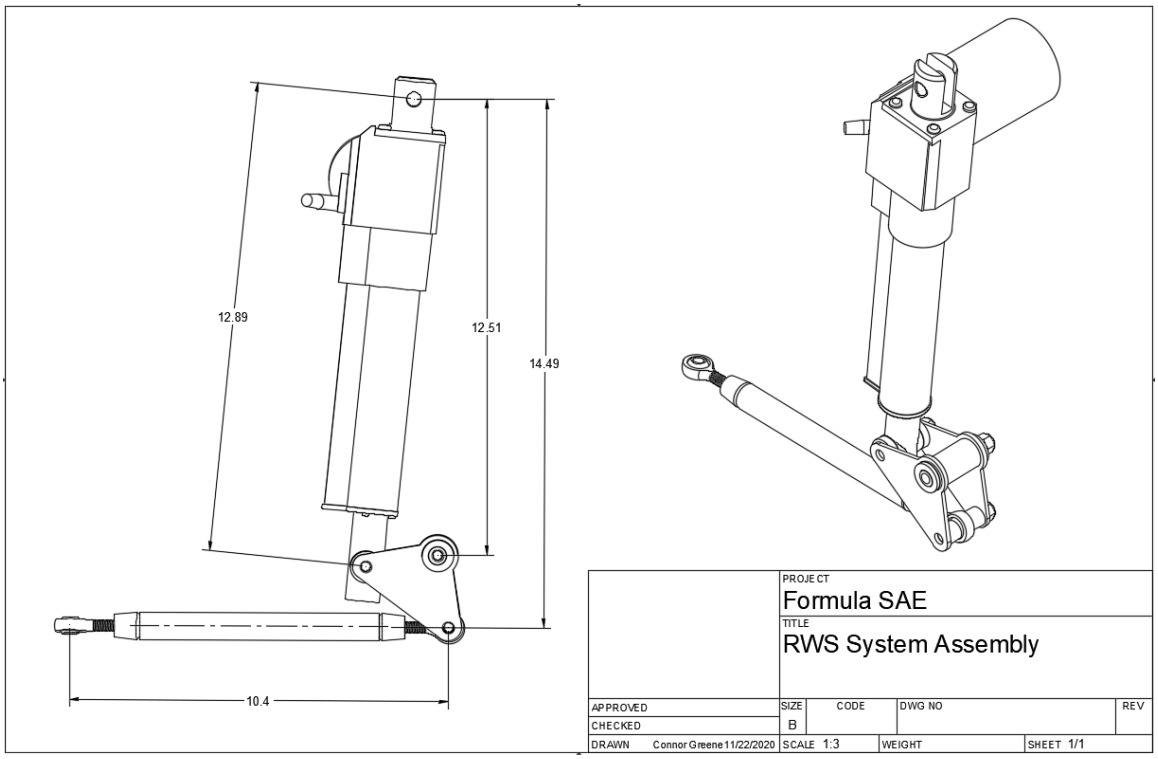

Figure 20: Dimensioned Drawing of RWS System Assembly.

Sheet metal will be used to construct the mounting tabs as well as the body of the rocker. We will use the waterjet to cut the profiles which will then be welded to the spacer cylinders on the rocker. Bushings will be purchased from McMaster-Carr and press-fit into the rocker. The tie rods will have McMaster-Carr weld-nuts and heim joints which are left- and right-hand threaded pairs as noted in Figure 19. This will allow us to adjust the length of the tie rod by twisting the body in one direction.

Analyzing the Design with Finite Element Analysis

Finite element analysis (FEA) is a method of predicting how a model reacts as a whole to various physical effects such as stress and displacement. A mesh breaks down the model into a finite number of smaller pieces known as elements. Predicting the behavior of each element, in turn, predicts the behavior of the model. Constraints and loads can be applied to simulate the environment. Computers are efficient at predicting behavior by analyzing mesh data. An FEA stress analysis was performed on the rear upright of the current car to see the effect of tire interaction. A more extreme case was considered in determining the loads applied as a precaution. 9000 N was applied in the vertical direction, 6000 N radially to where the wheel hub would attach and 6000 N laterally. The results of the study produced a model showing where the stress was concentrated. The most significant amount of stress, 36.78 MPa, occurred at the ends. With a safety factor over 7, the upright is not expected to fail under the extreme load case.

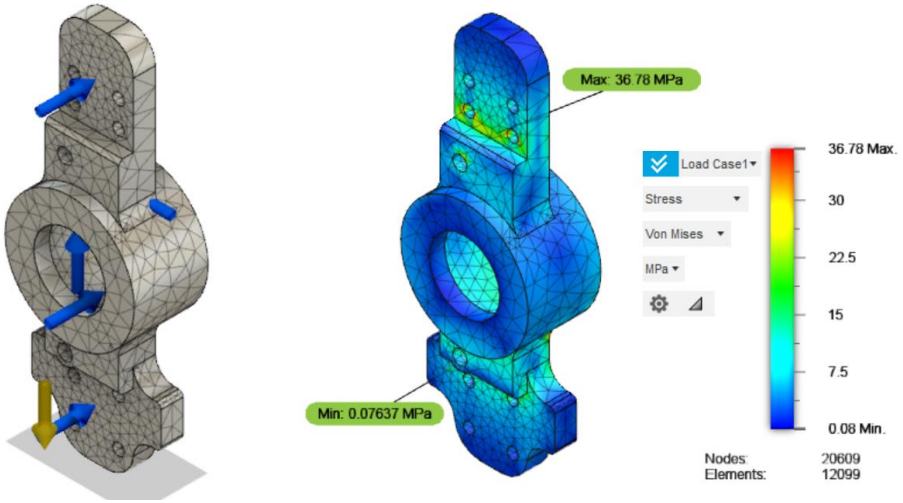

Figure 21: Rear upright with loads applied and the subsequent stress simulation.

Another stress analysis was performed on the rocker to see if it would be able to withstand the force output of the linear actuator. The maximum expected load was 300 lbs which was applied vertically to one end of the plates. The most amount of stress occurred around the bolt holes in the plates and was calculated to be 40.01 MPa. With a factor of safety of 5.1, the rocker is expected to be able to withstand the maximum force output.

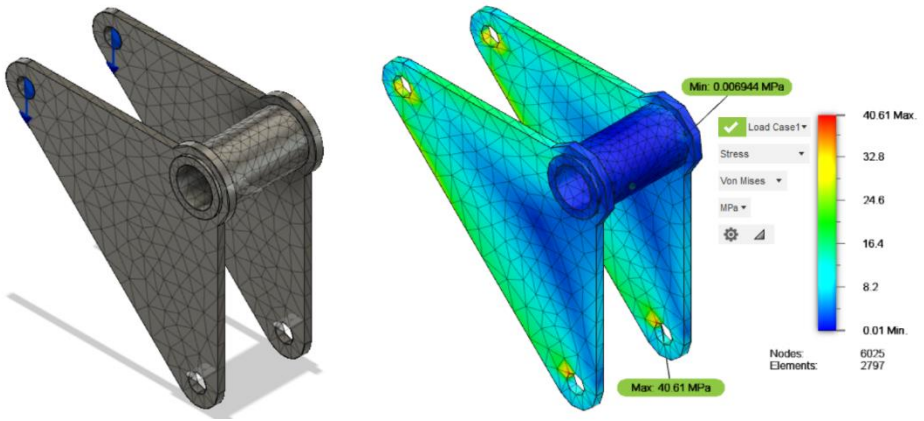

Figure 22: Rocker with loads applied and the results for the subsequent stress simulation. The left image shows the rocker CAD with the FEA mesh overlaid on top. The right image depicts the results of the FEA stress simulation highlighting the minimum and maximum points of stress measured in the component.

Electronics and Controls Design Overview

Developing the Controls Algorithm to Achieve the Desired Steering Performance

Once the desired high speed and low speed steering performance of the vehicle was determined, the team worked on designing the algorithm that would result in this performance using Matlab and Simulink. To start, the inputs and outputs of the system were identified and the controls algorithm was broken down into four main sections: the input signal section, the steering geometry section, the fail safe check section, and the control loop section. The inputs for the system include the steering rack potentiometer signal, the kill switch signal, and the vehicle's wheel RPM signals from its two rear wheels and the outputs of the system are the desired PWM voltage signals to actuate the right and left rear linear actuators.

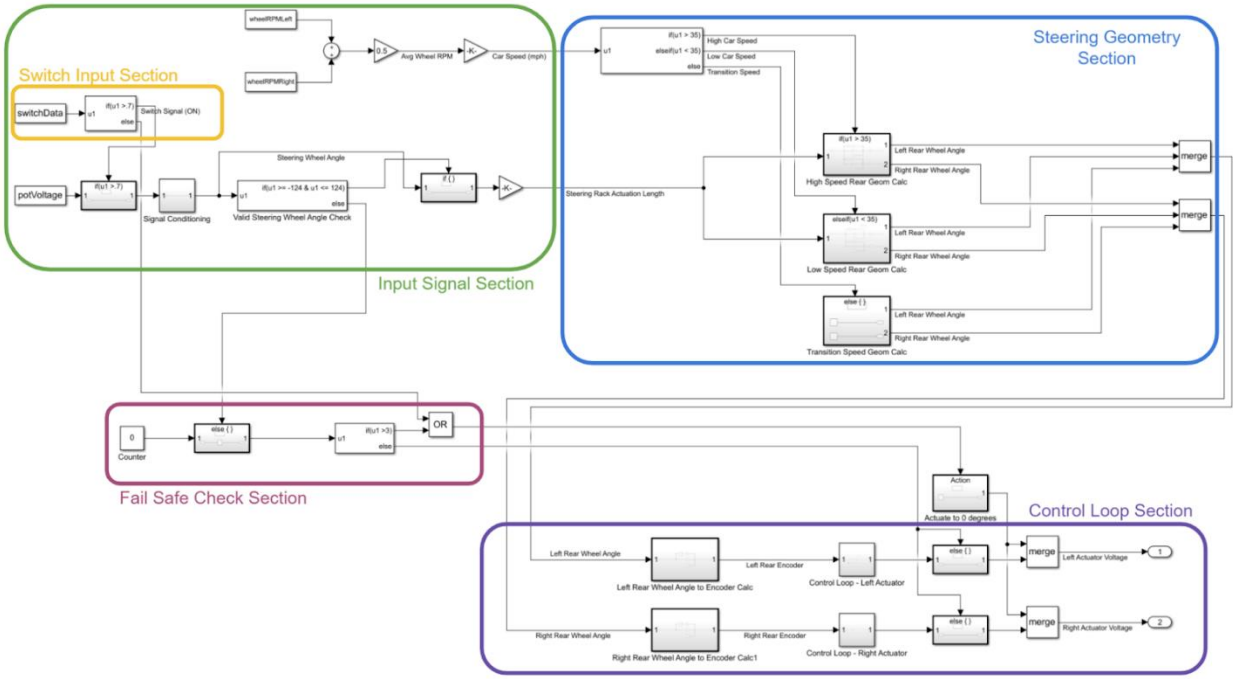

Figure 23: Overall System Block Diagram. This image shows the overall block diagram representation of the vehicle's control system algorithm. This algorithm takes in the steering rack potentiometer signal, the kill switch signal, and the vehicle's wheel RPM from its two rear wheels as inputs and outputs the voltage signals required for the left and right rear wheel linear actuators in order to actuate the rear wheels to their desired angles. It is organized into four main sections: the input signal section, the steering geometry section, the fail safe check section, and the control loop section.

As shown in Figure 23 above, the first section is the input signal section that takes in input from the kill switch, the steering rack potentiometer, and the vehicle's wheel RPM sensors and outputs the car speed and steering rack actuation length. This section is responsible for converting the voltage signal from the steering rack potentiometer into a steering rack actuation length value that can then be used in the steering geometry section, conducting input validation to ensure that the potentiometer signal being received is a valid value, and calculating the vehicle's speed based on the average of the RPM signals from the vehicle's rear wheels. This section also works with the fail safe check section to determine whether or not this supplemental rear wheel power steering system should be active by checking if either the kill switch is off or if the steering rack potentiometer has read too many invalid values. If either of these cases occurs, the system will turn off resulting in the rear wheels being actuated back to their neutral position.

After calculating the vehicle's current speed and steering actuation length, the steering geometry section then uses these two inputs to determine the vehicle's desired rear left and right wheel angles. To do so, the algorithm first determines if the vehicle speed is high, low, or at the transition and then feeds the steering rack actuation length to the appropriate speed's geometry calculation block (see Figures 24, 25, and 26). As determined previously, at high speeds, the vehicle will have Parallel costeer geometry where both rear wheels are actuated to the same steering angle (see Figure 24). At low speeds, the vehicle will have Ackermann countersteer geometry we calculate using a predetermined relationship between steering rack actuation length and rear wheel angles. Since the relationship for each of the rear wheels is different, different

gains are used in the calculation as shown in Figure 25. Finally, at the vehicle's transition speed, the left and right rear wheels will be actuated to a zero degree angle, or to their neutral positions, which results in no rear wheel power steering assistance at this speed (Figure 26). This allows the vehicle to have a simultaneous transition from Ackermann to Parallel steering geometry and from countersteer to costeer. Since the competition limits the motion of the rear wheels to a maximum of 6 degrees, each of these geometry calculation blocks uses a Simulink saturation block to prevent the desired rear wheel angle signals from being more than 6 degrees away from the neutral position.

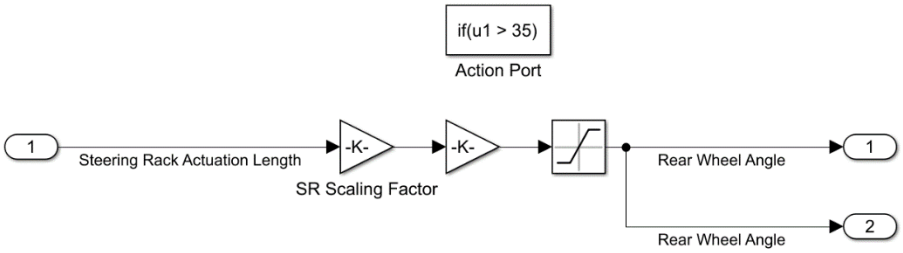

Figure 24: High Speed Geometry Calculation Block Diagram. This image shows the calculation of the desired left and right rear wheel angles from the left and right front wheel angles if the car is at a high speed using Parallel costeer steering geometry. The equations are based off of our steering geometry CAD sketches.

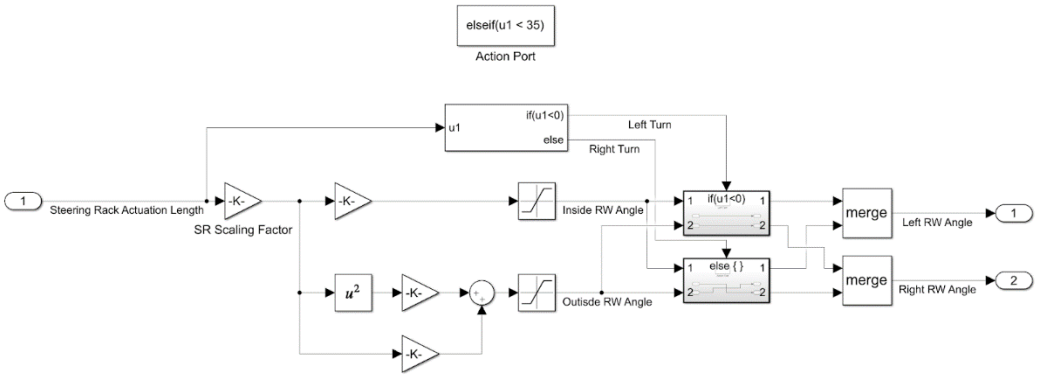

Figure 25: Low Speed Geometry Calculation Block Diagram. This image shows the calculation of the desired left and right rear wheel angles from the left and right front wheel angles if the car is at a low speed using Ackermann countersteer steering geometry. The equations are based off of our steering geometry CAD sketches.

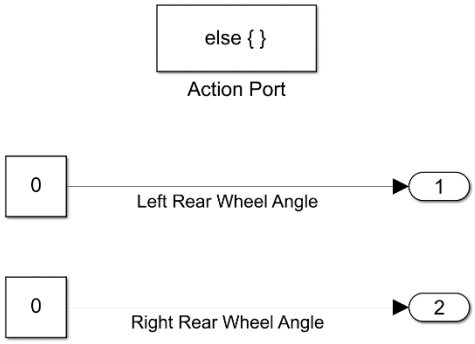

Figure 26: Transition Speed Geometry Calculation Block Diagram. This image shows the calculation of the desired left and right rear wheel angles from the left and right front wheel angles if the car is at the transition speed, resulting in the rear wheels being actuated to their neutral position (0 degrees of rear wheel steering).

To calculate the high speed and low speed geometry equations that relate the steering rack actuation length to the rear wheel angles, a coded script was used in conjunction with CAD sketches of 2D views of our steering geometry. Since our Fusion 360 CAD software's API has a built-in ability to run Python scripts, we used Python to write our script to allow us to interface with and iterate quickly through different dimensions in our CAD sketches. Using this script, we iterated through different rear wheel angles from -6 to +6 degrees and saved the corresponding steering rack actuation length. Finally, we plotted these points in Excel and found the best fit curve for the relationship between the rear wheel angle and the steering rack actuation length and the corresponding equations. Since only a small portion of the steering rack length was used in a 1:1 ratio between the front wheels and rear wheels for ±6 degrees of rear wheel steering angle, we wanted to be able to scale the inputs to these equations. This would allow us to have the rear wheels change their steering angle over a larger range of the steering rack's actuation. In order to allow for accurate scaling of the steering rack actuation input, when determining the best fit curves for the relationship between steering rack actuation length and rear wheel angle, we set the intercept of the best fit curve to run through the origin. As shown in Figure 27, the resulting best fit curves were linear relationships for outside wheel angle at low speeds and the rear wheel angles at high speeds and a second degree polynomial relationship for the inside wheel angle at low speeds.

Figure 27: Delta of Rear Wheel Angle vs Actuation of Steering Rack for left and right rear wheels at low speed and high speeds.

Between the steering geometry section and the control loop section, the desired rear wheel angles are converted into desired encoder position values using a conversion value determined from our rear wheel steering CAD assembly. As explained within the **Mechanical Design Overview** section, the rocker (and thus rotary encoded) rotates 1.36° for every one degree of wheel steering angle. These signals are then used in this algorithm's last section, the control loop section. In this section, the desired encoder position values are put through two separate control loops which each output the required PWM voltage signal to actuate their corresponding actuator to the desired positions. Looking more closely at the control loops, Figure 28 shows this loop is a negative feedback loop with the controller and the physical system modeled in the feedforward portion of the loop. The controller is designed to be a PID controller in which we will use the proportional component to tune the control system's response, the integral component to ensure that the control system response has zero steady state error, and the derivative component to counteract the lag in the system's feedback loop.

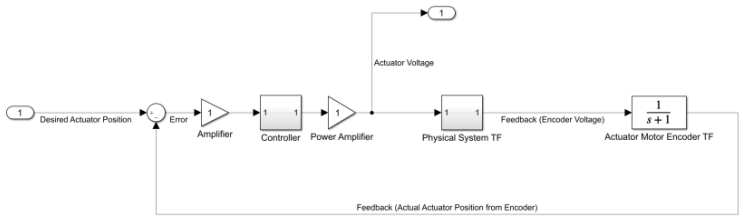

Figure 28: Control Loop Block Diagram. This image shows the control loop portion of the vehicle's control system algorithm which features a negative feedback loop with the desired actuator position as the input and the required voltage to actuate the actuator to its desired position as the output.

Interfacing with and Wiring of the Electronics

To measure the actuation length of our steering rack, we used a potentiometer mounted directly onto the bottom of our steering rack. This potentiometer converts the rotational motion of the pinion gear in the rack into a proportional voltage that we measure using our Arduino Mega microcontroller. Since the Arduino Mega has designated pins that can do analog-to-digital conversion (ADC), interfacing with the steering rack potentiometer was quite simple. The power and ground wires of the potentiometer were connected to 5V power and sensor ground respectively while the signal wire was connected to a ADC pin on the Arduino Mega. To read the voltage value of the potentiometer into the Arduino Mega, we used Arduino's analogRead() function that converts the 0-5V voltage to a value from 0-1023 proportionally.

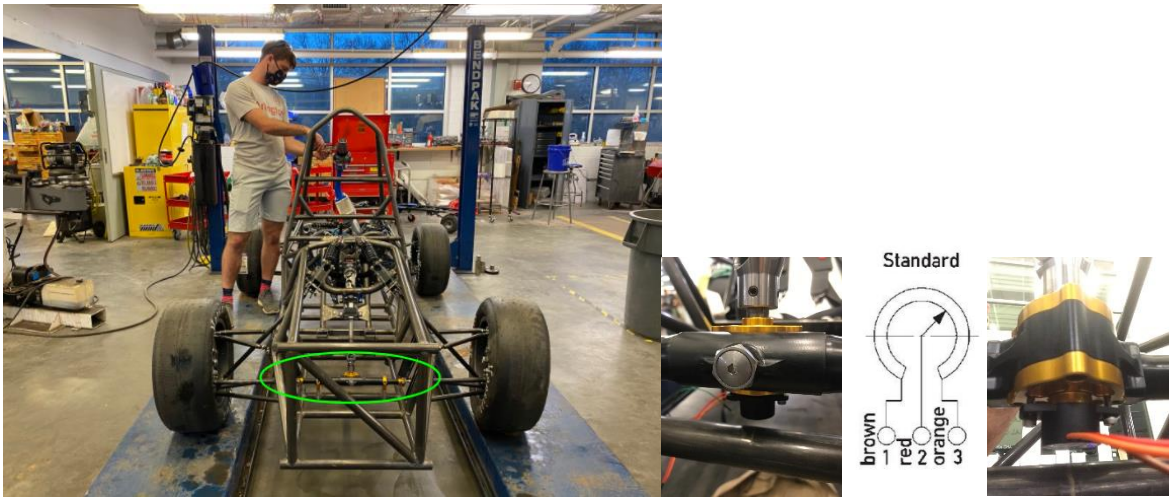

Figure 29: Front steering rack potentiometer placement, close-ups, and wiring diagram.

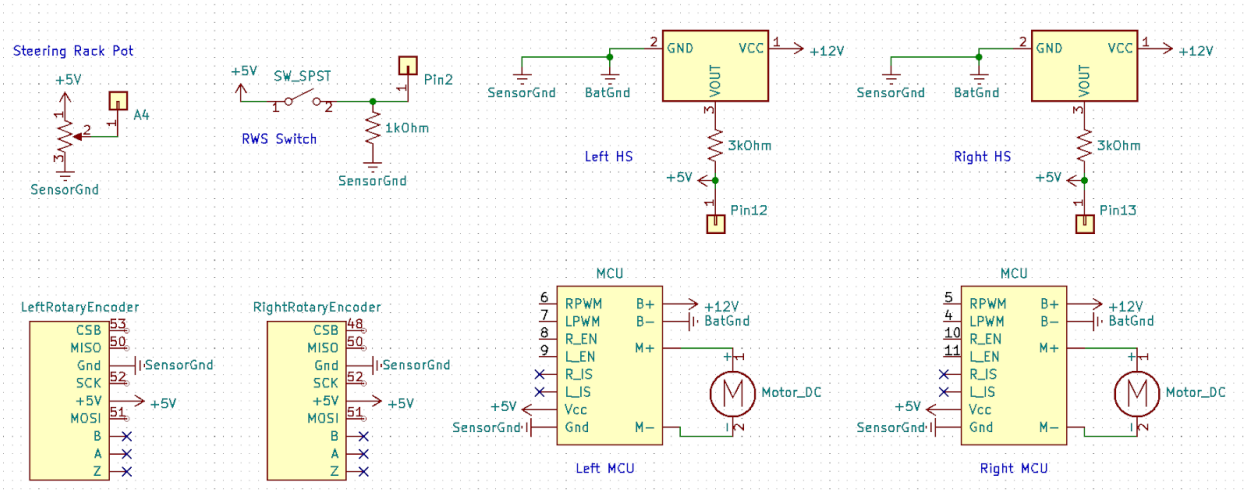

Figure 30: Wiring diagram for the steering rack potentiometer.

To read the vehicle speed from our hall effect sensors, we wired the sensors so that they received the necessary 12V power source, but only provided up to a 5V signal. As shown in the figure below, we limited the signal output of the hall effect sensor to 5V by using a pull-up resistor connected to the Arduino Mega's 5V power source. Since the hall effect sensor uses its grounding wire as a ground reference for its signal wire, we had to connect the battery ground with the sensor ground to ensure that the Arduino Mega and the hall effect sensors were using the same ground reference. As mentioned previously, the hall effect sensors are mounted above the rear axles' castle rings. As the rear axles rotate with the motion of the wheel, the hall effect sensors will measure the passing of the castle rings' teeth and can extrapolate the vehicle's wheel speed based on how many teeth the hall effect sensors measured passing by during a given period of time. Hall effect sensors work by sensing a change in the magnetic field surrounding it and as the teeth of the castle rings pass underneath it, the hall effect sensors' signals get pulled low. This pull to a low signal is what the Arduino measures and counts using digitalRead() to determine how fast the vehicle's wheels are moving.

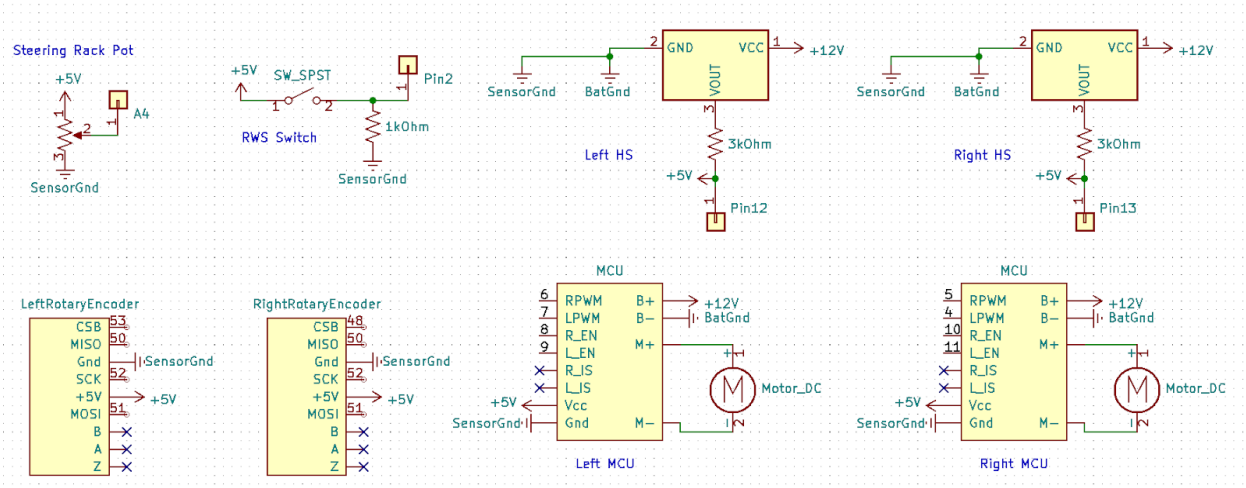

Figure 31: Wiring diagram for the left and right hall effect sensors.

To control the linear actuators, we used BTS7960 motor control units with integrated H-bridges to simplify the wiring. We chose this particular motor control unit because it's input voltage range included the 12V operational voltage of our actuators and because it allowed for forward and reverse pulse width modulation (PWM) motion control in a compact packaging. Since the Arduino Mega has designated pins capable of producing a PWM signal if given a value from 0-255, we elected to use those pins as part of our wiring as shown in Figure 33. Then, to send a PWM signal through the Arduino Mega, we used the built-in Arduino function analogWrite(). Besides PWM inputs for the forward and reverse directions as well as the expected power and ground inputs, our chosen motor control units also have inputs for enabling forward and reverse motion as well as side current alarm outputs for the forward and reverse directions. To control the activation of the motor control units, we also connected the inputs for enabling forward and reverse motion (R_EN and L_EN) to digital output pins on the Arduino Mega as shown in Figure 33. For enabling the motor control units to send power to the actuators, we set the output of those pins to HIGH in the setup section of our code. Because we did not need to use the alarm outputs on the motor control units, we left those unconnected.

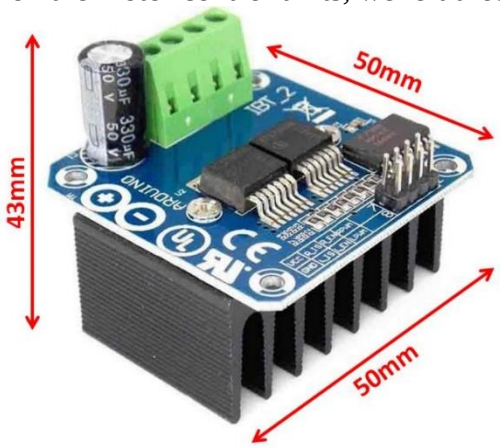

Figure 32: Motor control unit used to help control our linear actuators (Handson Technology, n.d.).

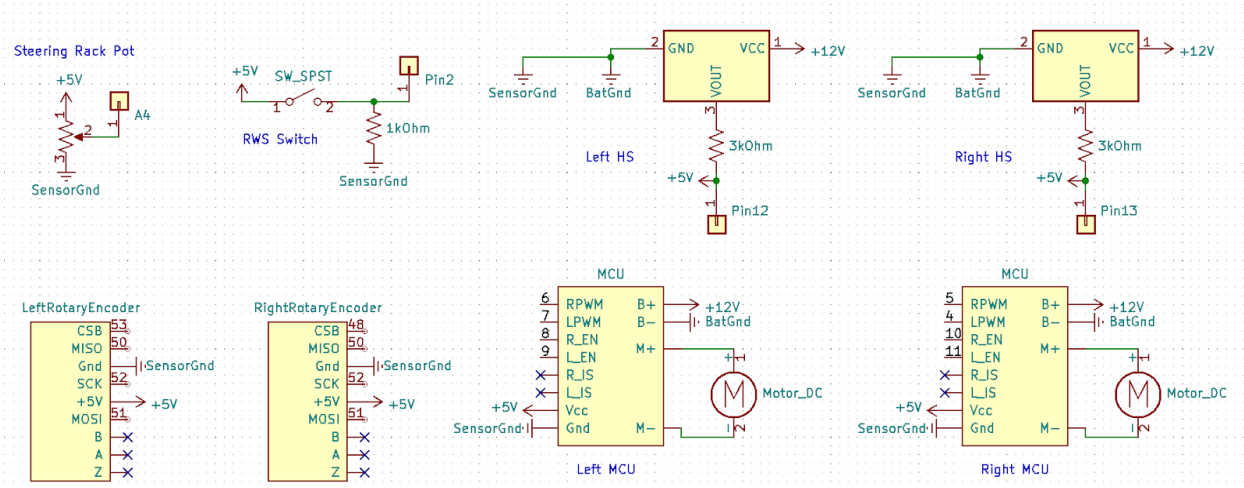

Figure 33: Wiring diagram for the left and right motor control units.

For our encoder, we chose to purchase the AMT 203-V quadrature encoder with absolute encoder capabilities programmed in. Since we wanted to be able to read our position definitively everytime, we chose to use the encoder's absolute encoder function. This required communicating with the encoder using Serial Peripheral Interface (SPI). Fortunately, the Arduino Mega has built-in pins for handling SPI communication. To read from both of our encoders, we used the designated SPI pins on the Arduino Mega and an additional digital pin for our second encoder's chip select. When programming the Arduino Mega to read from these encoders, we developed a helper method based on sample code provided by CUI Inc (Kelly, 2016).

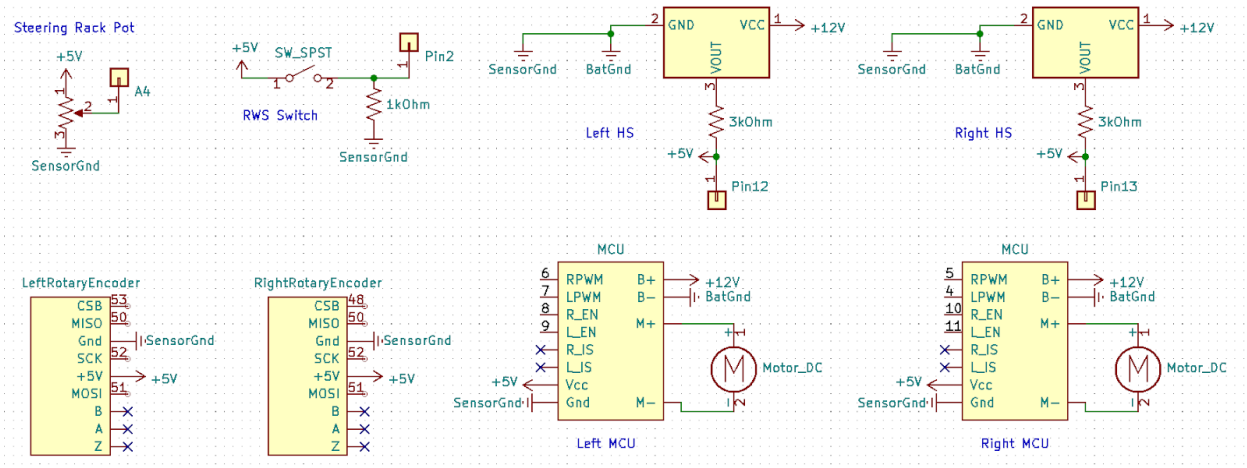

Figure 34: Wiring diagram for the left and right encoders.

To allow for the driver to activate and deactivate the supplemental rear wheel steering system, we also included a switch as part of our design. If this switch is on, our RWS system would be activated and the rear wheels would be actuated to their appropriate positions according to the driver's steering input. However, if this switch is ever turned off, our RWS system would be deactivated and the rear wheels would be actuated back to their neutral position. To read the signal from our switch, we wired it to 5V power and a digital input pin on

the Arduino Mega as shown in Figure 35. To ensure that the pin always read a low signal when the switch was open, we incorporated a pull-down resistor as part of the circuit.

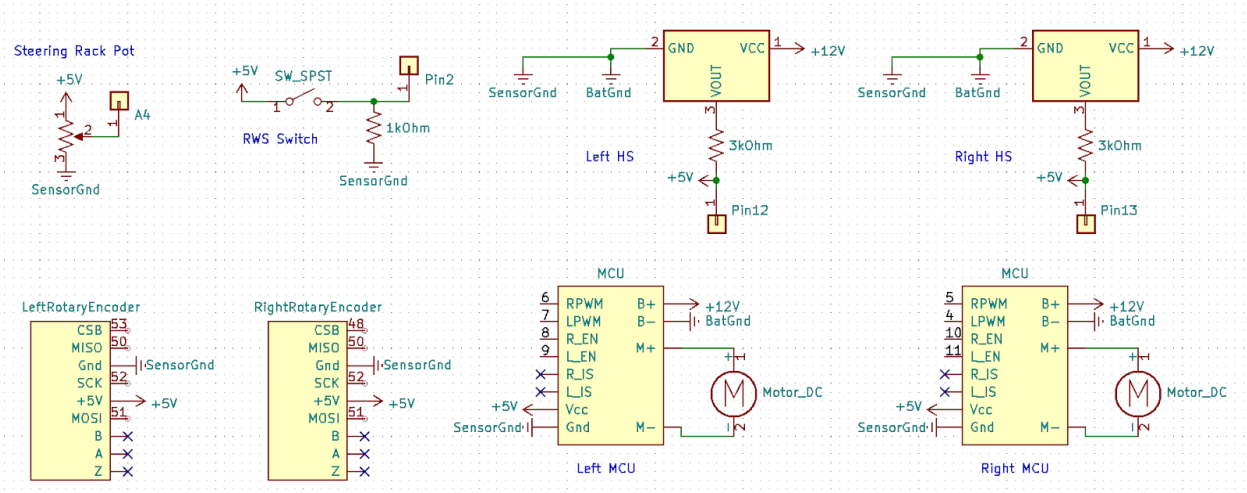

Figure 35: Wiring diagram for the RWS switch.

Implementing the Controls Algorithm on Arduino

The key to implementing the controls algorithm is the microcontroller used, the Arduino Mega. The block diagram developed in Matlab's Simulink provided the basic logic for the Arduino's code. With the setup of the block diagram in matlab to create the algorithm itself and do the tuning as needed, the Arduino can provide the implementation in two different methodologies. One method is to embed the Arduino capabilities within the Simulink model through the Simulink Support Package for Arduino (*Arduino Support from Simulink*, n.d.). The functionality of this setup allows the control logic of the block diagram to run on the Arduino board instead, which achieves a faster run rate for the controls algorithm and allows for faster sampling rates. The option the team went with was to code directly into Arduino's software system using Arduino IDE.

After developing helper methods to interface with each of the different sensors and actuators (steering rack potentiometer, hall effect sensors, encoders, and linear actuators), the next step was to directly code the pre-loop and main loop of our controls algorithm onto our Arduino Mega. For the pre-loop, we update all of our values for steering rack actuation length and vehicle speed based on our values from our steering rack potentiometer and our hall effect sensors. The pre-loop is also where we calculated our desired position values for our encoder based on these updated input values. Using the equations determined earlier for the relationship between steering rack actuation length and rear wheel angle, we first converted our updated steering rack actuation length to desired rear wheel angle. Then, using the conversion value we determined earlier for rear wheel angle to encoder angle, we convert our desired rear wheel angle to a desired encoder position. This desired encoder position value is the driving input for our control loop to move our linear actuators accordingly. For the main control loop, we used an Arduino library called Custom PID that helped simplify the coding of our PID control loop. With this library, we were able to define the values we wanted for our proportional, integral, and differential control as well as utilize its update function that the actual error measured in the system and returns adjusted PID error. This adjusted error is then used to determine the percent PWM to actuate each of the linear actuators in order for the actuators to best reach their desired

length. As more testing was conducted, these PID coefficients were adjusted so as to provide a better response time and performance for the actuators.

Failure Mode and Effects Analysis (FMEA)

FMEA was performed on our system to attempt to predict the components with the greatest risk of failure. Table III shows the results of the analysis, with each category being rated from 1 to 5, 5 greatest.

Table III

FMEA chart for each component in the RWS system

Component	Severity	Occurrence	Detection difficulty	RPN
Actuator	5	2	2	20
Steering angle sensor	2	1	1	2
Wheel speed sensor	3	2	3	18
Microcontroller	4	2	2	16
Wiring	4	2	1	8

As an overview, the components with the highest Risk Priority Number (RPN) are the actuators, the wheel speed sensors, and the microcontroller. The actuator has the highest severity because it is the only component which is an output from the system, and if it were to fail unexpectedly the driver's control would be unpredictable. The wheel speed sensor has the second highest RPN because it would be fairly difficult to detect when the vehicle is stationary, and there is no visual confirmation of its function unlike the potentiometer which can turn. The microcontroller has the third highest RPN because while it is the interface between all of the other components, it would be fairly easy to detect and there is a low chance of failure. In summary, the group must be cognizant of the possibility of failure in those components and impose contingency plans for each should they fail. This may be difficult with the actuators as they make up a large portion of our budget, but when designing our system and selecting our actuators, we used an absolute worst-case scenario actuation force.

Manufacturing

Manufacturing of the rear wheel steering system required use of machines in Lacy Hall, our machine shop at the University of Virginia, including the waterjet, 3-axis CNC mill, manual lathe, bandsaw, and TIG welder. The manufacturing processes for each component of the system are described in the subsections below.

Tie Rods

4130 steel tubing, outer diameter 0.75”, wall thickness 0.065”, were used as the tie rod’s main structural member. The tubes were cut to length on a bandsaw. Weld nuts purchased from McMaster Carr were welded to each end of the tube, with one of them being left-hand threaded and the other right-hand threaded. Matching threaded heim joints purchased from McMaster Carr were then screwed into the weld nuts.

Rockers

The 2D profile of the rocker was cut using a waterjet from 0.125” thick low carbon steel plate. The cylinder that houses the pivot bushings was CNC milled from a 1” outer diameter low carbon steel cylinder. The spacers allowing the tie rod’s heim joint to be mounted to the rocker were manually turned from 0.75” outer diameter low carbon steel cylinder stock. The bushing housing and rocker profile plates were then welded together, using the bushing sleeves and heim joints as pins to ensure geometric accuracy was maintained. The final rocker assembly is shown in Figure 36.

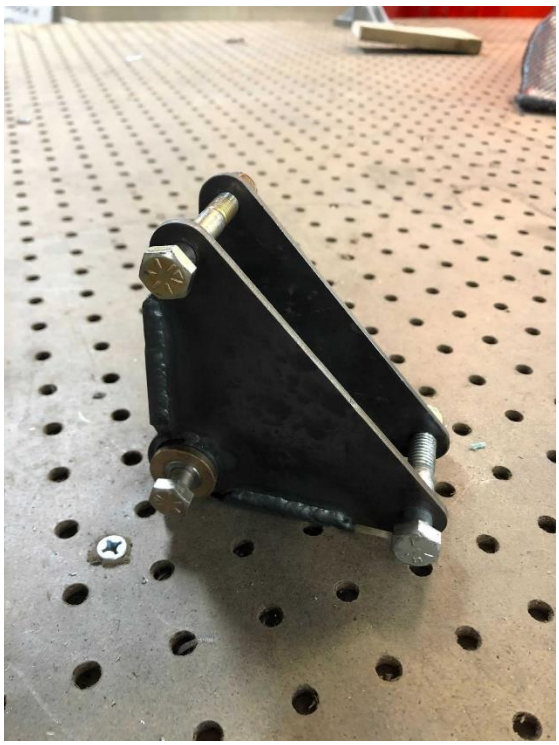

Figure 36: Rocker assembly with bushings and hardware

Actuator and Rocker Mounts

The profile of the mounts attaching the rocker to the frame were waterjet from 0.125” thick low carbon steel plate. The tabs were bent using a metal brake and then welded to the car’s

frame. Bump stops were also produced in a similar way and welded to the frame. The upper mount for the linear actuator needed to be 0.4 inches, so 0.5 inch thick steel plate was faced with the CNC mill, waterjet to final size and shape, and then welded to the frame. Figure 37 shows the welded mounting features on the frame with no components attached.

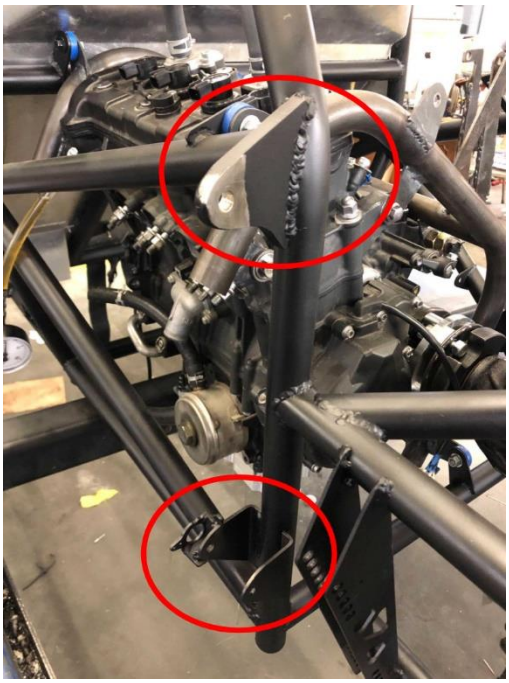

Figure 37: Welded mounting tabs for the rocker and linear actuator

Electronics Board

A custom circuit board was designed using a solderable busbar board and header pins. After iteratively testing our circuit board design using a breadboard to ensure all the wiring was correct (see Figure 38), we then transferred the design onto our solderable busbar board as shown in Figure 39.

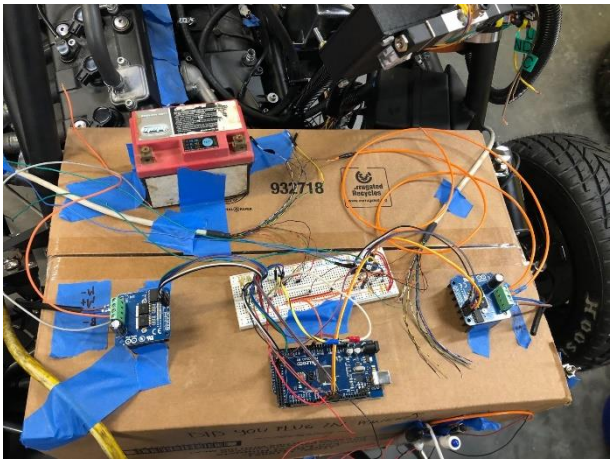

Figure 38: Breadboard set-up of our custom circuit board. This set-up was used to iteratively test each of our separate components' wiring.

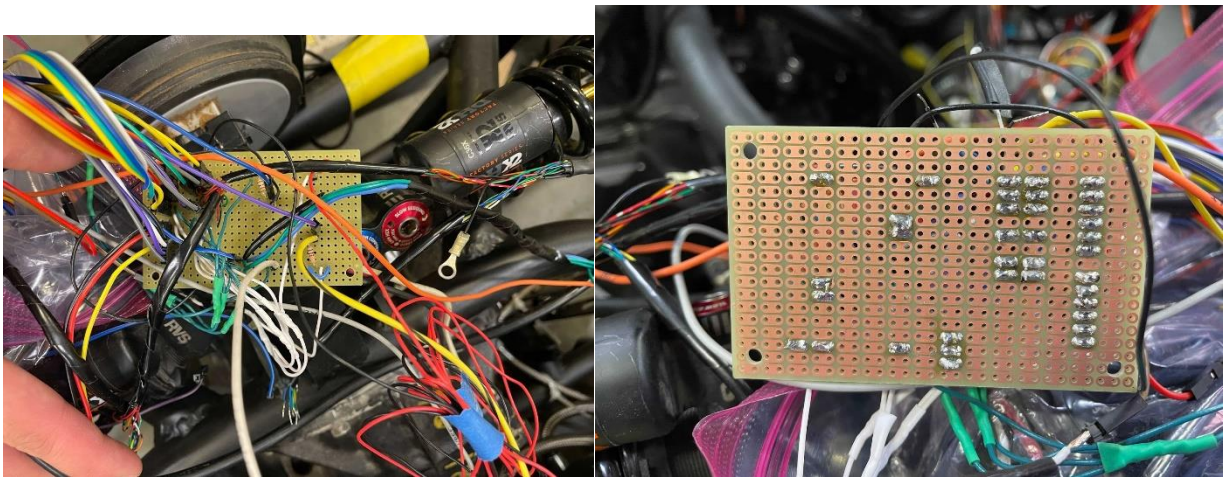

Figure 39: Custom circuit board design. Top view (left) and bottom view (right)

Challenges

The team encountered several challenges when manufacturing the RWS assembly. Most notably, distortion experienced in welding the rocker led to a far greater amount of tacks necessary than would be expected. Using hardware as aligners as explained above was necessary to ensure the parts would line up again once the part had cooled down. Another challenge was maintaining consistency across both assemblies: since tabs were "floating" on frame members, jigs were necessary to make sure they were placed at the right height and angle. Overall we were able to deal with the challenges quickly and effectively, resulting in a smoothly actuating mechanical system.

Testing Plan

Controls Algorithm Testing Plan

For the controls system, we hoped to test our controls algorithm through simulation both with real-world data and hypothetical, edge-case scenario data to ensure the robustness of the controls algorithm. To collect real-world input data, the team would have recorded data from the steering rack potentiometer and vehicle wheel RPM sensors while a driver conducts practice laps both under normal circumstances and under scenarios with rapid steering changes. This would help test how the controls system performs under real-world operating conditions as well as determine how good the signal conditioning portions of the system are at reducing the noise in the input signals. To test edge-case scenarios for system robustness, the team would have developed hypothetical input data for the steering rack potentiometer and vehicle wheel RPM sensors. This hypothetical data would help test how the controls algorithm will react to various invalid input signals and other potential hardware or software errors. Unfortunately, our team ran into time constraints with this project and was unable to complete this portion of our testing plan.

Whole System Testing Plan

The steering system will be tested dynamically once it is installed on the FSAE car. Testing will be broken into two categories: low vehicle speed and high vehicle speed performance. Low speed performance of the steering system will be quantitatively evaluated by slowly driving or pushing the car through a corner at maximum steering actuation. The turning radius of the car wheel then be measured from the centerpoint of the turn. The test will be

conducted both with the electronic rear wheel steering system activated and with the system deactivated. Turning radius achieved with and without the rear wheel steering system activated will then be compared.

The high vehicle speed test will measure the car's ability to make an agile high speed lateral "lane change" on a course similar to that shown below in Figure 40. The vehicle will be driven though the course both with and without the rear wheel steering system activated. Vehicle speed during each test will be recorded and will continue to be increased until the vehicle hits a cone marking the course boundaries. The maximum speed achievable without traveling outside the prescribed course will be compared between the tests done with and without the rear wheel steering system activated to determine the high speed performance benefits of the rear wheel steering system.

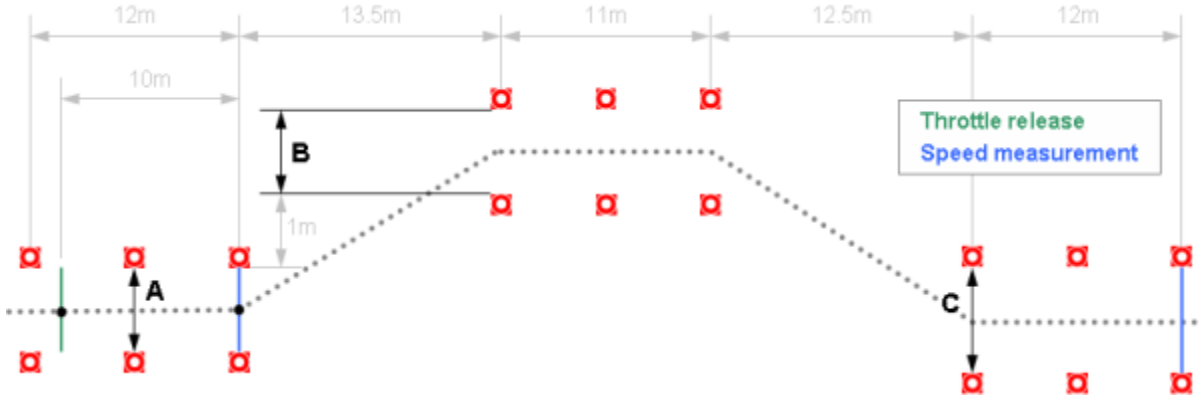

Figure 40: ISO Double Lane Change Test (ISO, n.d.).

Testing Results and Analysis

The effectiveness of the low speed steering geometry was tested by conducting a turning radius test both with and without RWS activated. The test was conducted a total of four times: twice with and twice without RWS activated. The average turning radius between the two tests is reported here. High speed performance has not yet been tested due to testing and tuning of our FSAE car's engine not aligning with this project's timeline. The low speed turning radius test setup can be seen in Figure 41. The frame of the vehicle was aligned to be parallel with a string marking a constant datum defining the starting position of the car. Yellow tape was also used to mark the centerline of the car's rear axles and the middle of the car to ensure consistency between each test.

Figure 41: Turning radius test starting setup.

For each test, the steering wheel was turned completely to the left and held at this position for the duration of the test. The vehicle was slowly rolled around a 180 degree arc beginning and ending along the string taped to the ground shown in Figure 42. To quantify the effectiveness of the RWS system, the turning radius test was conducted both with and without RWS activated. Without RWS activated, the vehicle's turning radius was 3.38 m. Figure 42 also shows the vehicle's path, marked with yellow tape, during this test without RWS engaged.

Figure 42: Turning radius test without rear wheel steering. (3.38 m turning radius).

With rear wheel steering activated, the vehicle's turning radius is 2.89 m. The vehicle's path with rear wheel steering engaged is marked with blue tape in Figure 43.

Figure 43: Turning radius test with rear wheel steering (blue tape marks path with rear wheel steering engaged). (2.89 m turning radius)

A 14.5% decrease in the vehicle's turning radius was achieved by the rear wheel steering system utilizing the low speed geometry. A close-up of the end of the vehicle's path with and without rear wheel steering activated is shown in Figure 43. While this 14.5% decrease in turning radius is not the 20% decrease our team was looking to achieve, this decrease is still substantial and will greatly improve vehicle agility and speed during low speed maneuvers. A much larger decrease in turning radius could be achieved if the rear wheels were able to be actuated beyond the ±6° of wheel angle allowed by the FSAE competition rules.

Figure 44: Close up view showing vehicle path with rear wheel steering activated (blue) and without RWS activated (yellow).

While care was taken to ensure consistency between tests, a more robust testing procedure would have increased accuracy. Specifically, it was difficult to position the vehicle in the exact same location at the beginning of each test. As shown in Figure 43, the blue (RWS activated) path initially swings out in a larger radius than the yellow no RWS path, thus indicating that the car was slightly misaligned relative to the string datum between the tests. Accuracy could have been improved by taking greater care to initially align the car before each test, and wheel casters could have been used to more easily manipulate the car into a consistent starting position. In total, this RWS system adds roughly 10 pounds to the vehicle, and thus we remained within our goal of adding less than 12 pounds to the net vehicle weight. We did not meet our weatherproofing and shock proofing goals due to time constraints and the nature of our prototype testing setup.

Table IV

Comparison of our Results and our System Requirement Goals

Specification	Plan	Actual	Did we meet it?
Low Speed Turning Radius	Decrease current vehicle low speed turning radius by 20% (currently 3.3m)	Low speed designed and works, 20% decrease in turning radius was not achieved	✗
High Speed Maneuverability	Improve high speed maneuverability, measure with "lane change" or obstacle avoidance test	High speed designed and works (test to be completed)	✓
Stay within $950 budget	Stay in budget and consider costs when purchasing items	Spent approx. $900	✓
Fail Safe System	Incorporate a fail-safe system to return rear wheel angles to 0 in case of unacceptable sensor values or driver choice	Fail safe system designed and functionality confirmed	✓
Weather/Shock Proofing	Be weatherproof (IP54+) and shockproof	Products rated as low as IP 43, but is plenty weatherproof for our competition	✗
Weight	Add < 12 lbs to the vehicle weight	Approx. 10 lbs added	✓

Project Schedule

The initial plan for the project was to spend fall semester focused on research and conceptual development for the RWPS system, and in the spring semester start to manufacture and install the hardware of the car then test the system as a whole before the FSAE competition in May (as seen in Figure 45). This whole process was estimated to take twelve weeks each semester to complete, for a total of 24 weeks for the entire project. This schedule allowed for some leeway in case the team came across any difficulties. Alongside manufacturing, the controller was to be designed and programmed in addition to the wiring and programming of the individual sensors during the spring.

During the fall semester, major decisions were made in regards to the design and the preliminary design was drawn and assembled in CAD. The team was on track in terms of our pre-determined schedule throughout the semester, meeting deadlines as needed, with slight delays caused by design iterations later on in the semester when problems arose with actuator mounting. At the end of the fall semester, a new schedule was drafted up with more detail to better represent the plan for the spring semester, as seen in Figure 46. The start of the spring semester followed the plan to some accuracy, but issues arose with delays in the coding and manufacturing of the vehicle as a whole. This, paired with an unequal distribution of responsibilities, led to the schedule being shifted in certain areas, with controller tuning and full-system testing not starting until the start of May. Overall, despite not staying completely on schedule, the RWPS system was still completed and tested by the end of production on May 7th.

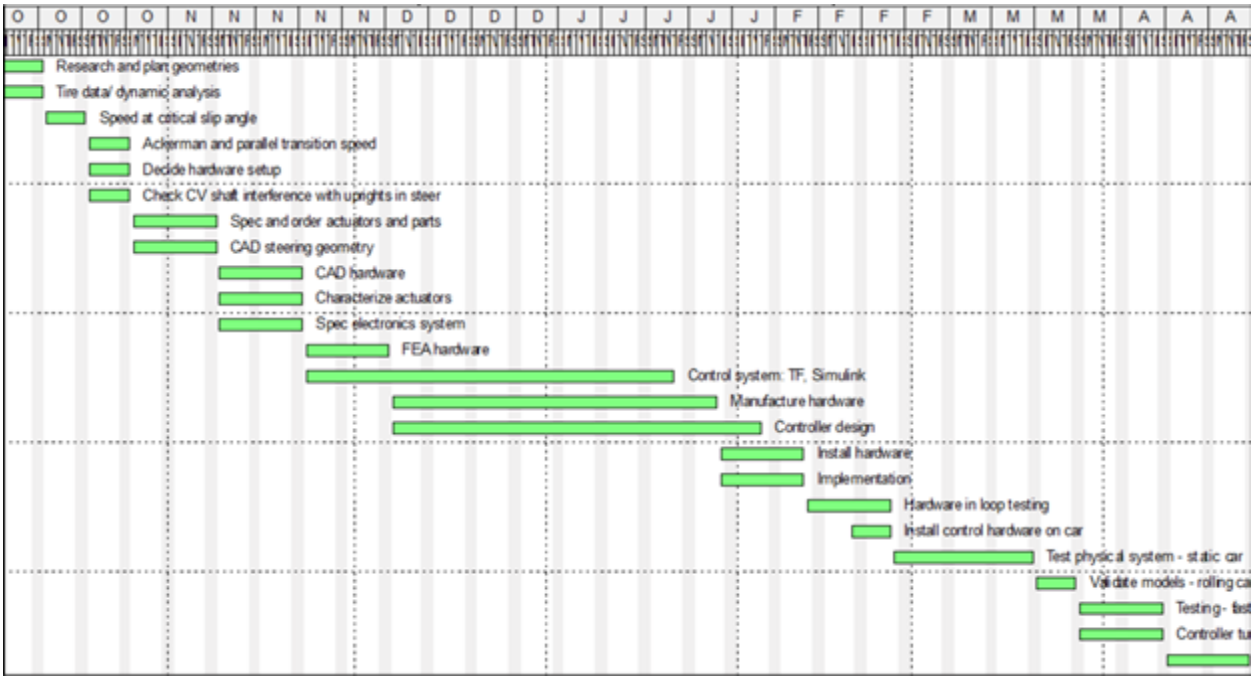

Figure 45: Whole Year Gantt Chart for Virginia Motorsports' Supplemental Rear Wheel Power Steering Project.

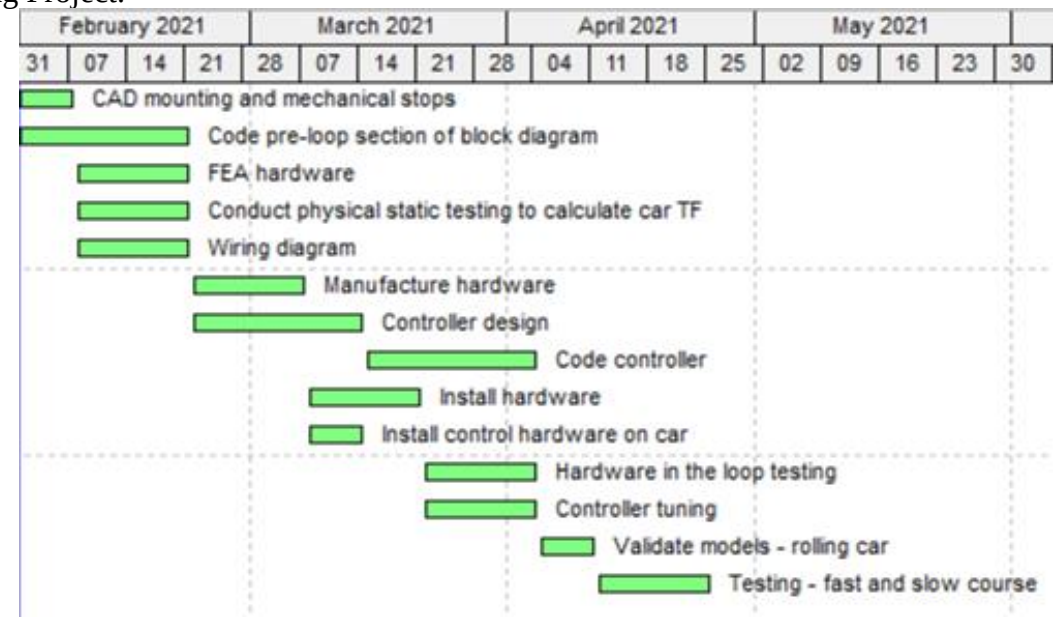

Figure 46: Updated Spring Semester Gantt Chart for Virginia Motorsports' Supplemental Rear Wheel Power Steering Project.

Project Budget

The main sources of funding for this project come from the Capstone Discretionary Funding ($450) and the Student Engagement Funding ($500), totaling up to $950. The Student Engagement Funding was applied for by the members of the Capstone group under the name of the Virginia Motorsports organization and the Capstone Discretionary Funding is allotted to the group by the university. A large portion of the budget will go towards the electronic linear

actuators, the PA-03 Actuators provided by Progressive Automation, and another larger portion of the budget will go towards other necessary electronics such as the microcontroller, steering rack potentiometer, encoders, and hall effect sensors. The remaining budget will be mainly used additional electronics supplies including the busbar boards for manufacturing our custom circuit boards as well as other various hardware and materials needed to construct the system as shown in Table V.

Table V

Virginia Motorsports' Budget for Supplemental Rear Wheel Power Steering Project

Assets				Amount
	Capstone Discretionary Funding			$450.00
	Student Engagement Funding			$500.00
Total Assets				$950.00
Expenses		Quantity	Per Part Cost	Cost
	PA-03 Actuators	2	$137.33	$274.66
	Arduino Mega Microcontroller	1	$64.38	$64.38
	Steering Rack Potentiometer	1	$145.33	$145.33
	Hall Effect Sensors	2	$47.48	$94.96
	Encoders	2	$50.31	$100.62
	Encoder Cables (purchased from different locations due to availability and price)	2	-	-
		1	$51.18	$51.18
		1	$15.80	$15.80
	Toggle Switch	1	$4.81	$4.81
	Busboards and Header Pins (more expensive due to additional shipping costs)	1	$14.31	$14.31
	Stock Metal, Bolts, Nuts	1	$104.75	$104.75
Total Cost				$870.80
Margins				$79.20

Future Work

There are many opportunities for improvement regarding our supplemental rear wheel steering system. One of the main aspects of our system that can be improved is the optimization of our PID controller. Instead of tuning the controller based on only real-world testing, we would

recommend characterizing the physical system and using Simulink to help optimize the PID coefficient values through iterative testing and simulation. This is something we wanted to implement, but unfortunately didn't get a chance to accomplish due to time constraints. Another opportunity for improvement would be to explore other controller designs beyond PID such as using root locus to develop a controller and evaluate their performances.

In terms of the mechanical portion of our RWS system, many improvements could be made on reducing the play or slop in the assembly as well as improvement alignment. In particular, one of the biggest issues we had with regards to manufacturing was warping of our welded components due to the heat generated by the welding process. By developing more accurate methods for manufacturing the different components, the team would be able to greatly improve the alignment of encoder and actuator mounts as well as decrease the amount of backlash in the system as a whole. Both of these improvements would help increase the accuracy of the rear wheel actuation with regards to instruction from the Arduino Mega microcontroller.

Lastly, we would recommend conducting tests on the system as a whole with regards to its functionality and durability under various conditions. This would include conducting the high speed functionality test we were unable to complete due to time constraints as well as running it through several FSAE endurance race set-ups. By testing the system under race-like conditions, the team would be able to analyze its performance and durability much more accurately. Overall, while we were able to produce a working prototype of our supplemental rear wheel steering system, there are still many different ways to improve the system for future work.

References

Ackerman Steering. (2016). Retrieved October 31, 2020, from http://datagenetics.com/blog/december12016/index.html

Andersen, C. (2013). *Modeling, analysis and testing of the Steering system in a Formula student car FS_UiS2013*. University of Stavanger. https://uis.brage.unit.no/uis-xmlui/bitstream/handle/11250/183062/Andersen%2C%20Christoffer%20Leidland.pdf?sequence=1&isAllowed=

Arduino Support from Simulink. (n.d.). Retrieved November 4, 2020, from https://www.mathworks.com/hardware-support/arduino-simulink.html

Arvind, V. (2013). Optimizing the turning radius of a vehicle using symmetric four wheel steering system. International Journal of Scientific & Engineering Research, 4(12).

Bremer, E., & Landemoo, V. (2018, May). *Mechanisms for rear wheel steering on a Formula Student car*. KTH Royal Institute of Technology - School of Industrial Engineering and Management. https://www.diva-portal.org/smash/get/diva2:1217656/FULLTEXT01.pdf

Brown, K. (2014). The University of Western Ontario team's FSAE car [Photograph]. In *Virginia Motorsports Formula SAE 2019-2020 Google Drive*.

Control Tutorials for MATLAB and Simulink—PI Control of DC Motor Speed. (n.d.). Retrieved November 2, 2020, from https://ctms.engin.umich.edu/CTMS/index.php?aux=Activities_DCmotorB

Formula SAE. (2020). *Formula SAE Rules 2020.* https://fsaeonline.com/cdsweb/gen/DownloadDocument.aspx?DocumentID=1b6bda52-48d0-4286-931d-c9418165fd3e

General Motors Quadrasteer Technology. (n.d.). Retrieved October 31, 2020, from https://gmauthority.com/blog/gm/general-motors-technology/gm-chassis-suspension-technology/gm-quadrasteer/

Handson Technology. (n.d.). *BTS 7960 Motor Control Unit with Dimensions* [Photograph]. Handsontec.com. https://www.handsontec.com/dataspecs/module/BTS7960%20Motor%20Driver.pdf

How to read a linear actuator encoder with Arduino—Shift Automation. (n.d.). Retrieved November 24, 2020, from https://shiftautomation.com/arduino-read-linear-actuator-encoder

ISO. (n.d.). ISO Lane Change Test. Retrieved November 23, 2020, from https://www.vehico.com/index.php/en/applications/iso-lane-change-test

KAZ Technologies. (2014, February). *KAZ Technologies Steering Rack* [Photograph]. https://www.kaztechnologies.com/fsae/steering-rack/

Kelly, J. (2016, August 8). *AMT20 Series - Arduino Sample Code.* CUI Devices. https://www.cuidevices.com/product/motion/rotary-encoders/absolute/modular/amt20-series

Linear Actuator PA-03. (n.d.). Progressive Automations. Retrieved November 24, 2020, from https://www.progressiveautomations.com/products/linear-actuator

McRae, J., & Potter, J. (2019). *Design Consideration of an FSAE Steering System.* Washington University in St. Louis. https://openscholarship.wustl.edu/mems500/94/

Milliken, W. F., & Milliken, D. L. (1995). Race car vehicle dynamics. Warrendale, PA, MI: SAE International.

Sparrow, A., Rowsell, P., & Wisniewski, T. (2016). *Four-Wheel Steering.* Washington University in St. Louis. https://openscholarship.wustl.edu/mems411/49/